

RESEARCH ARTICLE

View Article Online

View Journal | View Issue



Cite this: *Inorg. Chem. Front.*, 2021, **8**, 4507

Reductive silylation of polyoxovanadate surfaces using Mashima's reagent†

Sourav Chakraborty and Ellen M. Matson *

Here, we present the first example of reductive silylation for oxygen defect formation at the surface of a polyoxometalate. Upon addition of 1,4-bis(trimethylsilyl)dihiropyrazine (Pyz(SiMe₃)₂) to [V₆O₇(OMe)₁₂]^{1−}, quantitative formation of the oxygen-deficient vanadium oxide assembly, [V₆O₆(OMe)₁₂]^{1−} was observed. Substoichiometric reactions of Pyz(SiMe₃)₂ with the parent cluster revealed the mechanism of defect formation; addition of 0.5 equiv. of Pyz(SiMe₃)₂ to [V₆O₇(OMe)₁₂]^{1−} results in isolation of [V₆O₆(OSiMe₃)(OMe)₁₂]^{1−}. This reactivity was extended to reduced and oxidized forms of the cluster, [V₆O₇(OMe)₁₂]ⁿ (n = 2−, 0), revealing the consequences of modifying the oxidation states of remote transition metal ions on the stability of the siloxide functional group, and thus the extent of reactivity of the cluster surface with Pyz(SiMe₃)₂. The work offers a new understanding of the mechanisms of surface activation of reducible metal oxides *via* reductive silylation, and reveals new chemical routes for the formation of oxygen atom vacancies in polyoxometalate ions.

Received 25th July 2021,
Accepted 18th August 2021
DOI: 10.1039/d1qi00920f
rsc.li/frontiers-inorganic

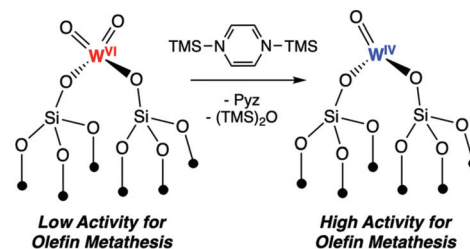
Introduction

Transition metal oxides are materials used widely in industrial catalysis, as both catalyst supports, and active species invoked in oxygen atom transfer reactions.^{1–4} Seminal contributions based on *in situ* and *in operando* analyses have revealed that the reactivity of these materials is dependent on the degree of surface activation, typically through the formation of oxygen atom defect sites.^{5–10} In accordance with the Mars van-Krevelen mechanism,^{11,12} oxygen atom vacancy formation results in the formation of a low-valent transition metal ion at the surface of the material poised for small molecule activation.^{5,9,13–15} Typically, surface activation of metal oxides is accomplished *via* high temperature and/or treatment of the material under H₂ or CO, rendering catalysts active only under energy-intensive conditions.^{16–18} This has motivated researchers to understand the mechanism and local electronic consequences of defect formation, toward the development of new routes to facilitate surface activation.⁵

With relevance to the aforementioned challenges, recent work has highlighted the use of silyl transfer reagents (*e.g.* 1,4-bis(trimethylsilyl)dihiropyrazine, Pyz(SiMe₃)₂) to facilitate the reduction of thermodynamically robust metal oxygen bonds (Fig. 1).¹⁹ The reductive power of this silyl transfer reagent,

referred to as “Mashima's reagent”, was first reported in 2014 by Mashima and coworkers as a salt-free route for the formation of low-valent, transition metal compounds.²⁰ In 2016,

Activation of WO₃/SiO₂ with Mashima's Reagent



Proposed structure for reduced W atom at SiO₂ surface

This Work: Mechanism of Surface Activation of POV-alkoxide Clusters with Mashima's Reagent

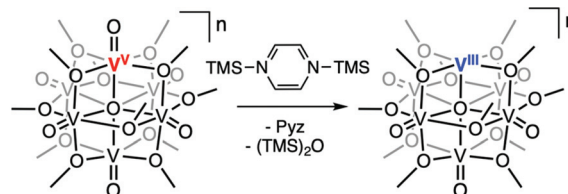


Fig. 1 Overview of presented work. Top of figure highlights seminal contributions from Mashima & Copéret invoking surface activation of M=O (M = Mo, W) fragments for improved olefin metathesis reactivity of silica supported transition metal ions;²¹ bottom of figure highlights the extension of these findings in this work, emphasizing the role of electronic communication within a network of redox active metals in facilitating O-atom defect formation.

Department of Chemistry, University of Rochester, Rochester, NY 14627, USA.

E-mail: matson@chem.rochester.edu

†Electronic supplementary information (ESI) available: ¹H NMR (500 MHz, CD₃CN, 21 °C) of compounds, LC-MS analysis of pentanes washes of reductive silylation reactions to detect formation of Pyz and (Me₃Si)₂O. See DOI: 10.1039/d1qi00920f

Mashima and Copéret reported the treatment of WO_3/SiO_2 materials with $\text{Pyz}(\text{SiMe}_3)_2$ at 70 °C, resulting in the formation of an active olefin metathesis catalyst *via* the reduction of surface $\text{W}^{\text{VI}}=\text{O}$ moieties.²¹ This result eliminated the necessity of harsh operating conditions previously required for catalyst activation in WO_3/SiO_2 (>350 °C), translating to a more efficient and general heterogeneous catalyst for olefin metathesis. Later, the same research team extended this reductive chemistry to the activation of molybdenum oxide moieties supported at silica surfaces, resulting in the identification of a heterogeneous catalyst for olefin metathesis operative at room temperature.²²

The seminal findings of Mashima and Copéret highlight the relevance of Mashima's reagent for surface activation in transition metal oxide systems through oxygen atom vacancy formation.^{21,22} However, in the case of the aforementioned articles, the redox-active tungsten and molybdenum oxide moieties are bound to redox-inactive supports, rendering the transition metal ions electronically isolated from other redox-active metal centres. These single site catalysts lack the delocalized electronic profiles relevant to bulk reducible metal oxides, prompting further exploration into surface activation of materials composed of redox-active metal centres capable of electronic communication.

Polyoxometalates are polynuclear inorganic molecular assemblies, comprised of transition metal oxoanions linked together through bridging oxygen atoms.^{23–25} The elemental composition and delocalized electronic structure of these clusters has resulted in their use in studies focused on elucidating mechanisms of substrate activation at metal oxide surfaces.^{26–28} Over the past five years, our research team has developed synthetic routes for the surface activation of polyoxovanadate-alkoxide clusters, making use of these nanoscopic, redox active assemblies as molecular models for the surface chemistry of reducible metal oxides.²⁹ Like plenary polyoxometalate motifs, Lindqvist-type polyoxovanadate-alkoxide clusters possess rich redox profiles.^{30–33} However, all twelve surface bridging oxide moieties are replaced by alkoxide ligands, increasing the solubility of polyoxovanadate-alkoxides in organic solvent and lim-

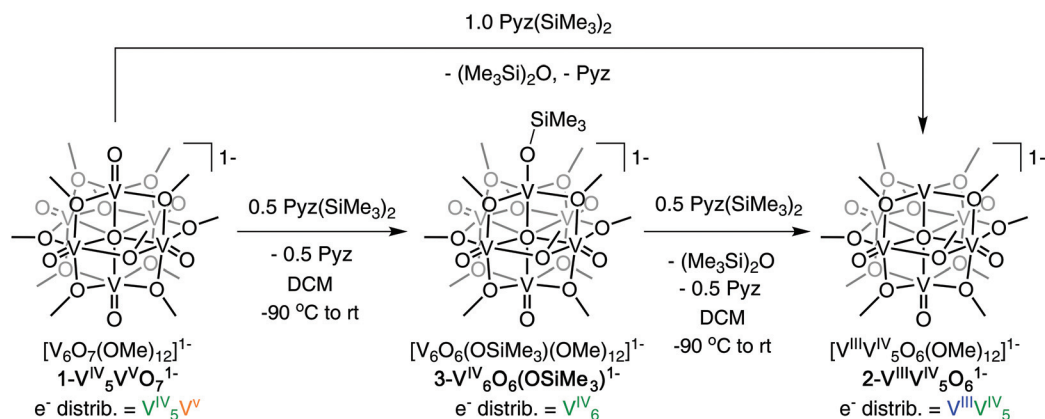
iting reactivity to the more electrophilic, terminal oxide moieties ($\text{V}=\text{O}$; O_t = terminal oxygen atom). These bridging alkoxide ligands also support low oxidation states of the cluster. The five distinct charge states of the assembly that have been reported to date are each composed of mixed-valent vanadyl ions (*e.g.* $\text{V}_{6-x}^{\text{IV}}\text{V}_x^{\text{V}}$; $x = 0-4$) and have been characterized as Robin and Day Class II delocalized systems.³⁴ Collectively, the distinct physicochemical properties of polyoxovanadate-alkoxide clusters provide opportunities for our team to probe the reactivity of metal oxide assemblies under rigorously anhydrous conditions, using spectroscopic techniques reserved for homogeneous compounds.^{35–37}

Toward understanding the mechanism and electronic consequences of surface reductive silylation in redox-active transition metal oxides, we report the reactivity of a series polyoxovanadate-alkoxide clusters with Mashima's reagent. Activation of terminal $\text{V}=\text{O}$ bonds at the surface of the cluster is accomplished through addition of 0.5 or 1 equiv. of $\text{Pyz}(\text{SiMe}_3)_2$ to $[\text{V}_6\text{O}_7(\text{OMe})_{12}]^{1-}$ ($n = 2-, 1-, 0$). We present electronic studies that probe the oxidation state distribution of vanadium ions within the cluster, detailing the role electronic communication plays in facilitating oxygen atom vacancy formation in these clusters.

Results and discussion

Reactivity of $[\text{V}_5^{\text{IV}}\text{V}^{\text{V}}\text{O}_7(\text{OMe})_{12}]^{-1}$ with Mashima's reagent

We opted to begin our studies of reductive silylation with polyoxovanadate-alkoxide clusters using the monoanionic variant of the vanadium oxide assembly, $[\text{V}_6\text{O}_7(\text{OMe})_{12}]^{1-}$ ($1\text{-V}_5^{\text{IV}}\text{V}^{\text{V}}\text{O}_7^{1-}$; Scheme 1). This cluster serves as an ideal starting point, as the oxidation state distribution of vanadium ions in the Lindqvist assembly includes a single, high-valent vanadium centre (V^{V}) that can be reduced by two electrons upon formation of an oxygen atom defect site. Our research team has previously reported the use of this charge state of the polyoxovanadate-alkoxide cluster to isolate an assembly bearing a single oxygen atom vacancy and a $2e^-$ reduced



Scheme 1 Reactivity of $1\text{-V}_5^{\text{IV}}\text{V}^{\text{V}}\text{O}_7^{1-}$ with various equiv. of $\text{Pyz}(\text{SiMe}_3)_2$.

vanadium centre, $[\text{V}_6\text{O}_6(\text{OMe})_{12}]^{1-}$ ($2\text{-V}^{\text{III}}\text{V}_5^{\text{IV}}\text{O}_6^{1-}$, ox. state distrib. = $\text{V}^{\text{III}}\text{V}_5^{\text{IV}}$).³⁸ We hypothesized that similar deoxygenation of the cluster surface *via* $\text{V}=\text{O}$ bond cleavage would be observed following addition of $\text{Pyz}(\text{SiMe}_3)_2$ to $1\text{-V}_5^{\text{IV}}\text{V}^{\text{V}}\text{O}_7^{1-}$.

Addition of 1.0 equiv. of $\text{Pyz}(\text{SiMe}_3)_2$ to $1\text{-V}_5^{\text{IV}}\text{V}^{\text{V}}\text{O}_7^{1-}$ at low temperature resulted in a colour change to red-brown, suggesting formation of the oxygen-deficient assembly (Scheme 1). Following work up, characterization of the product *via* ^1H NMR spectroscopy indicated formation of $2\text{-V}^{\text{III}}\text{V}_5^{\text{IV}}\text{O}_6^{1-}$ in excellent yield (94%; Fig. S1†). Analysis of pentanes washes of the crude reaction mixture by liquid chromatography mass spectrometry (LC-MS) confirmed formation of pyrazine and hexamethyldisiloxane as the by-products of deoxygenation (Fig. S2 and S3†).

In principle, surface activation of metal oxo fragments *via* reductive silylation occurs *via* two distinct silyl transfer steps, proceeding through a metal-siloxide intermediate. In recent work, our laboratory has reported the formation of a siloxide functionalized polyoxovanadate-alkoxide cluster, $[\text{V}_6^{\text{IV}}\text{O}_6(\text{OSiMe}_3)(\text{OMe})_{12}]^{1-}$ ($3\text{-V}_6^{\text{IV}}\text{O}_6(\text{OSiMe}_3)^{1-}$), *via* addition of trimethylsilyl trifluoromethylsulfonate to the fully-reduced, dianionic variant of the Lindqvist clusters, $[\text{V}_6^{\text{IV}}\text{O}_7(\text{OMe})_{12}]^{2-}$. Notably, this compound is identical in formula to the proposed product of a single silyl radical transfer to the mono-anionic polyoxovanadate-alkoxide cluster surface ($1\text{-V}_5^{\text{IV}}\text{V}^{\text{V}}\text{O}_7^{1-}$). Toward the elucidation of whether $3\text{-V}_6^{\text{IV}}\text{O}_6(\text{OSiMe}_3)^{1-}$ serves as an intermediate in oxygen atom vacancy formation, we next explored substoichiometric addition of Mashima's reagent to $1\text{-V}_5^{\text{IV}}\text{V}^{\text{V}}\text{O}_7^{1-}$. The drop-wise addition of frozen slurries of 0.5 equiv. of $\text{Pyz}(\text{SiMe}_3)_2$ to $1\text{-V}_5^{\text{IV}}\text{V}^{\text{V}}\text{O}_7^{1-}$ in dichloromethane was performed (Scheme 1). Analysis of the crude reaction mixture by ^1H NMR spectroscopy reveals formation of pyrazine and complete consumption $1\text{-V}_5^{\text{IV}}\text{V}^{\text{V}}\text{O}_7^{1-}$ (Fig. S4†). Three new paramagnetically shifted and broadened resonances were observed at 27.50, 24.12 and -9.79 ppm, matching those previously reported for the siloxide-functionalized species, $3\text{-V}_6^{\text{IV}}\text{O}_6(\text{OSiMe}_3)^{1-}$ (Fig. S5†).

We have previously described the characterization of $3\text{-V}_6^{\text{IV}}\text{O}_6(\text{OSiMe}_3)^{1-}$,³⁹ however with relevance to the mechanism of surface activation by silyl radicals reported here, we present the infrared and electronic absorption spectroscopies of this cluster in comparison to $1\text{-V}_5^{\text{IV}}\text{V}^{\text{V}}\text{O}_7^{1-}$ and $2\text{-V}^{\text{III}}\text{V}_5^{\text{IV}}\text{O}_6^{1-}$ (Fig. 2). Two transitions diagnostic of the oxidation state of the Lindqvist cluster were observed in the IR spectrum of $3\text{-V}_6^{\text{IV}}\text{O}_6(\text{OSiMe}_3)^{1-}$ ($\nu(\text{O}_b\text{-CH}_3) = 1044\text{ cm}^{-1}$, $\nu(\text{V}=\text{O}) = 955\text{ cm}^{-1}$; Fig. 2a). These values are within error of those reported for the fully-oxygenated polyoxovanadate-alkoxide, $1\text{-V}_5^{\text{IV}}\text{V}^{\text{V}}\text{O}_7^{1-}$ ($\nu(\text{O}_b\text{-CH}_3) = 1047\text{ cm}^{-1}$; $\nu(\text{V}=\text{O}) = 953\text{ cm}^{-1}$), suggesting minimal change in the distribution of electron density across the cluster core upon silylation. This result is unexpected, given that silyl radical transfer to the surface of the vanadium oxide assembly results in the formal injection of an electron into the cluster core, as evidenced by the change in oxidation state distributions of the vanadium oxide assemblies following silylation (e.g. $1\text{-V}_5^{\text{IV}}\text{V}^{\text{V}}\text{O}_7^{1-}$: $\text{V}_5^{\text{IV}}\text{V}^{\text{V}}$; $3\text{-V}_6^{\text{IV}}\text{O}_6(\text{OSiMe}_3)^{1-}$: V_6^{IV}). Reduction of the single V^{V} ion of $1\text{-V}_5^{\text{IV}}\text{V}^{\text{V}}\text{O}_7^{1-}$ following

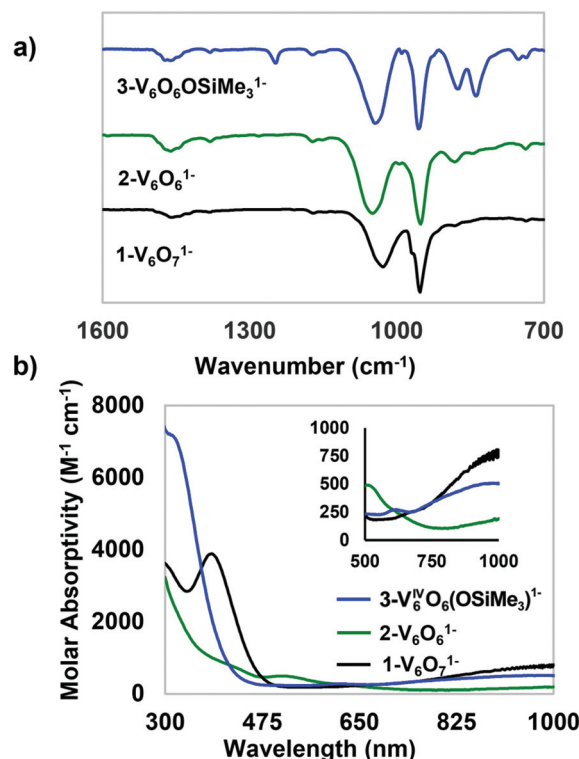


Fig. 2 Spectroscopic characterization of $1\text{-V}_5^{\text{IV}}\text{V}^{\text{V}}\text{O}_7^{1-}$, $2\text{-V}^{\text{III}}\text{V}_5^{\text{IV}}\text{O}_6^{1-}$, and $3\text{-V}_6^{\text{IV}}\text{O}_6(\text{OSiMe}_3)^{1-}$: (a) IR spectrum; (b) electronic absorption spectrum collected in acetonitrile at 21°C . The inset shows the low-energy region of the spectrum to more clearly illustrate IVCT bands.

addition of Mashima's reagent is more evident in comparing the electronic absorption spectra of the starting material and the silylated species; quenching of the intervalence charge transfer (IVCT) bands of $1\text{-V}_5^{\text{IV}}\text{V}^{\text{V}}\text{O}_7^{1-}$ is noted in the relatively featureless electronic absorption spectrum of $3\text{-V}_6^{\text{IV}}\text{O}_6(\text{OSiMe}_3)^{1-}$ (Fig. 2b). Taken together, these results suggest that silyl transfer affords reduction of a single vanadium ion (e.g. $\text{V}^{\text{V}}=\text{O} \rightarrow \text{V}^{\text{IV}}\text{-OSiMe}_3$), and that this reduction event remains localized to the site differentiated metal centre, with minimal impact on the charge distribution of the remaining vanadyl ions of the assembly.

The reactivity of polyoxometalates with silyl transfer reagents (e.g. Mashima's reagent) has not been reported. This fact is surprising, given the well-established ability of polyoxometalate clusters to negotiate cation-coupled electron transfer processes, effectively delivering an equiv. of "M" (M = Li, Na, K, Cs) or "H" to the cluster surface.^{40–43} In contrast, significant research effort has focused on the modification of the cluster surface through the organo-functionalization of polyoxometalates *via* reactivity with silylium ions. This work has leveraged the increased nucleophilicity of terminal oxide ligands of Lacunary polyoxometalate assemblies for the formation of bridging siloxide moieties at the surface of the cluster. Knoth and coworkers reported the first evidence of silylation in polyoxometalates,⁴⁴ resulting in the isolation of $[\alpha\text{-SiW}_{11}\text{O}_{39}\{\text{O}(\text{SiR})_2\}]^{4-}$ *via* addition of RSiCl_3 (R = Et, Ph,

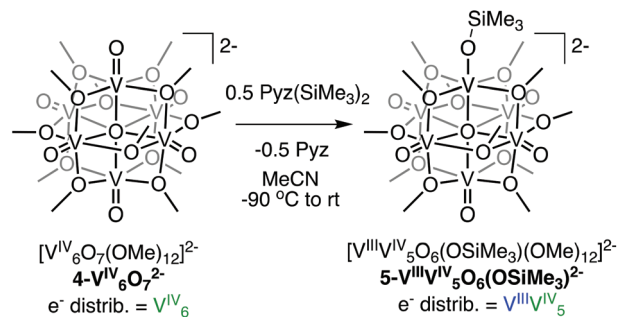
C_3H_5) in water. Since then, the functionalization of Lacunary polyoxometalates *via* addition of organosilanes has become a well-accepted strategy for the organo-functionalization of these metal-oxide assemblies, translating to a wide variety of siloxide-functionalized polyoxometalates.^{45–48}

The formation of *terminal* siloxide on the surface of polyoxometalates is quite unusual. This unique silylation of terminal oxo is evident in the niobium-substituted polyoxotungstates. Upon substitution of W^{VI} moieties with a Nb^V heteroatom in the inert, hexatungstate Lindqvist ion, the total charge of the polyoxometalate increases (e.g. $[W_6O_{19}]^{2-}$ to $[NbW_5O_{19}]^{3-}$). This supplemental charge is partially localized on the terminal oxygen atom bound to the Nb centre. The increased nucleophilicity of the $Nb=O$ bond enhances the reactivity of assembly with electrophiles such as silylium ions, resulting in selective $Nb=O$ bond activation at the site differentiated metal centre. Indeed, addition of *tert*-butyldimethylsilyl trifluoromethyl sulfonate to Lindqvist ion, $[Nb_2W_4O_{19}]^{4-}$ produces a heterometal-substituted polyoxometalate bearing a terminal siloxide ligand,⁴⁹ $[Nb_2W_4O_{19}Si(CH_3)_2C(CH_3)_3]^{3-}$. However, there is no evidence of direct silylation on $[NbW_5O_{19}]^{3-}$. Alternatively Lindqvist $[NbW_5O_{19}SiR_3]^{2-}$ ($R = Et, tBuMe_2, iPr, Ph$) can be synthesized by the reaction of $[NbW_5O_{18}]_2O^{4-}$ with silanols.⁵⁰

It is presumed that the formation of $2-V^{III}V_5^{IV}O_6^{1-}$, *via* addition of Mashima's reagent to $1-V^{IV}V^VO_7^{1-}$, proceeds through the isolated intermediate $3-V_6^IVO_6(OSiMe_3)^{1-}$ (*vide supra*). To confirm this proposed route for O-atom defect formation, 0.5 equiv. of $Pyz(SiMe_3)_2$ was added to $3-V_6^IVO_6(OSiMe_3)^{1-}$. The immediate colour change of the solution from green to red-brown suggested formation of the oxygen-deficient polyoxovanadate-alkoxide cluster. Conversion of the silylated assembly to $2-V^{III}V_5^{IV}O_6^{1-}$ was confirmed *via* 1H NMR spectroscopy (Fig. S6†). Cleavage of the siloxide functional group from the surface of the cluster following a second equiv. of $SiMe_3$ results in formation of $(Me_3Si)_2O$, as confirmed by LC-MS (Fig. S7†). These results confirm the proposed mechanism of oxygen atom defect formation *via* step-wise reductive silylation of a surface vanadyl ion with Mashima's reagent.

Reductive silylation of $[V_6^IVO_7(OMe)_{12}]^{2-}$

To investigate the role oxidation state distribution of the Lindqvist core plays in dictating the reactivity of the metal oxide assembly, we next explored the reactivity of $[V_6^IVO_7(OMe)_{12}]^{2-}$ ($4-V_6^IVO_7^{2-}$) with Mashima's reagent. In contrast to the mixed-valent polyoxovanadate-alkoxide, $1-V^{IV}V^VO_7^{1-}$ (ox. state distrib. = $V^{IV}V^V$), this reduced derivative of the cluster possesses an isovalent oxidation state distribution (V_6^{IV}). Slow addition of 0.5 equiv. of $Pyz(SiMe_3)_2$ to $4-V_6^IVO_7^{2-}$ results in a gradual colour change from teal to light green (Scheme 2). Analysis of the 1H NMR spectrum of the crude product (Fig. S8†) revealed a broad signal corresponding to the starting material ($\delta = 23.6$ ppm), and formation of a new product with three distinct paramagnetically shifted and broadened resonances ($\delta = -8.41, 22.75$, and 24.77 ppm). Previously, we have reported the synthesis of the dianionic form of the siloxide-functionalised assembly, accessed *via*



Scheme 2 Synthesis of $5-V^{III}V_5^{IV}O_6(OSiMe_3)^{2-}$; addition of $Pyz(SiMe_3)_2$ to $4-V_6^IVO_7^{2-}$.

reduction of $3-V_6^IVO_6OSiMe_3^{1-}$ with cobaltocene; the 1H NMR spectrum reported for $[V^{III}V_5^{IV}O_6(OSiMe_3)(OMe)_{12}]^{2-}$ ($5-V^{III}V_5^{IV}O_6(OSiMe_3)^{2-}$) matches that of the minor species formed following addition of Mashima's reagent to $4-V_6^IVO_7^{2-}$.³⁹

Compound $5-V^{III}V_5^{IV}O_6(OSiMe_3)^{2-}$ could be isolated from the starting material *via* extraction with tetrahydrofuran, albeit in low yield (4%). While integration of the 1H NMR spectrum of the reaction mixture suggested better conversion (Fig. S8†), similarities in the solubility of the compound with the starting material, coupled with the instability of $5-V^{III}V_5^{IV}O_6(OSiMe_3)^{2-}$ at room temperature, rendered isolation challenging.

In our original report, we described the spectroscopic characterization of $5-V^{III}V_5^{IV}O_6(OSiMe_3)^{2-}$, with attention paid to its relevance as a model for hydrogen atom uptake in vanadium dioxide.³⁹ Broadly, the electronic profile of $5-V^{III}V_5^{IV}O_6(OSiMe_3)^{2-}$ resembles closely that of the dianionic, fully-oxygenated precursor, $4-V_6^IVO_7^{2-}$. IR spectroscopy showed the expected broad transitions for $5-V^{III}V_5^{IV}O_6(OSiMe_3)^{2-}$ indicating retention of structural integrity of the Lindqvist core ($\nu(O_b-CH_3) = 1063\text{ cm}^{-1}$, and $\nu(V=O_t) = 939\text{ cm}^{-1}$) (Fig. 3a). The electronic absorption spectrum of $5-V^{III}V_5^{IV}O_6(OSiMe_3)^{2-}$ features weak transitions at 626 and 1000 nm, resembling those of $4-V_6^IVO_7^{2-}$ (Fig. 3b). However, it is worth noting that bond valence sum calculations performed *via* structural analysis suggest that the site differentiated vanadium centre generated upon addition of a silyl radical to a single vanadyl moiety is reduced ($V^{IV} \rightarrow V^{III}$), resulting in an oxidation state distribution assignment for $5-V^{III}V_5^{IV}O_6(OSiMe_3)^{2-}$ of $V^{III}V_5^{IV}$. Like that described for the addition of Mashima's reagent to $1-V^{IV}V^VO_7^{1-}$, addition of the silyl radical results in the reduction of the cluster core by a single electron.

Addition of subsequent equiv. of $Pyz(SiMe_3)_2$ to $5-V^{III}V_5^{IV}O_6(OSiMe_3)^{2-}$ does not result in the formation of an oxygen deficient Lindqvist ion. This is likely due to the fact that V^{II} centres are not expected to be stable in the oxygen-rich environment of the polyoxovanadate-alkoxide cluster. This result is consistent with both our previously described inability to remove an oxygen atom from the surface of $4-V_6^IVO_7^{2-}$,⁵¹ as well as the lack of reduction events observed in the cyclic voltammogram of $2-V^{III}V_5^{IV}O_6^{1-}$.³⁸ However, it is notable that despite the availability of five additional $V^{IV}=O_t$ moieties at the

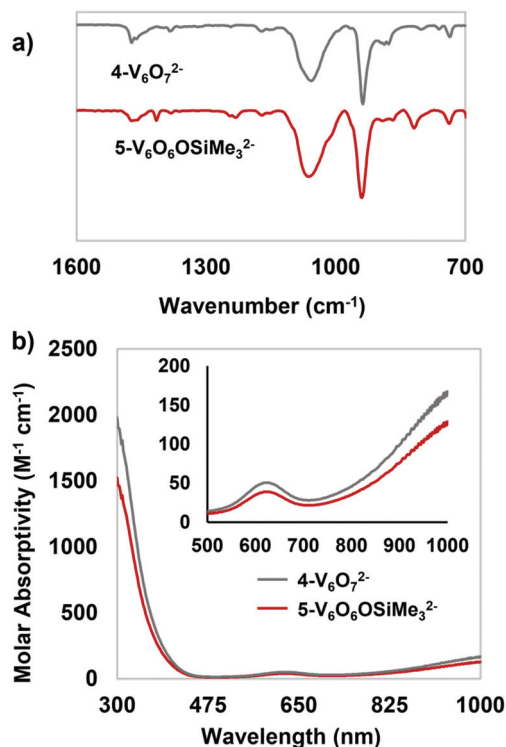


Fig. 3 Spectroscopic characterization of $4\text{-V}_6^{\text{IV}}\text{O}_7^{2-}$ and $5\text{-V}_6^{\text{III}}\text{V}_5^{\text{IV}}\text{O}_6(\text{OSiMe}_3)^{2-}$: (a) IR spectrum; (b) electronic absorption spectrum collected in acetonitrile at 21 °C. The inset shows the low-energy region of the spectrum to more clearly illustrate IVCT bands.

cluster surface, no additional reactivity with Mashima's reagent takes place. This is likely due to the increased nucleophilicity of the cluster surface upon the first silylation event, rendering subsequent additions of silyl radicals to the remaining surface $\text{V}=\text{O}$ moieties of the assembly thermodynamically prohibited.

Silyl radical transfer to the surface of $4\text{-V}_6^{\text{IV}}\text{O}_7^{2-}$ broadly resembles proton–electron co-doping processes recently reported for VO_2 (Fig. 4).^{52,53} The authors describe the hydrogenation of VO_2 in the presence of acid and a source of electrons (e.g. metal nanoparticle, ascorbic acid). These hydrogen atom doping events result in the reduction of V^{IV} ions to V^{III} , as observed by X-ray photoelectron spectroscopy, and concomitant formation of sub-surface O–H bonds within the material. If one considers the trimethylsilyl moiety to function as a “bulky hydrogen atom surrogate”, as has been reported recently by Ménard and co-workers,⁵⁴ the results described for the reactivity of $4\text{-V}_6^{\text{IV}}\text{O}_7^{2-}$ with $\text{Pyz}(\text{SiMe}_3)_2$ show striking similarities to the chemistry described above. The iso-valent oxidation state distribution of $4\text{-V}_6^{\text{IV}}\text{O}_7^{2-}$ (V_6^{IV}), and coordination geometries of individual vanadium centres (pseudo-octahedral), make the low-valent polyoxovanadate-alkoxide an intriguing model for bulk VO_2 , as demonstrated previously by our research group.^{55,56} Upon exposure of $4\text{-V}_6^{\text{IV}}\text{O}_7^{2-}$ to $\cdot\text{SiMe}_3$, reduction of vanadium is observed ($\text{V}^{\text{IV}} \rightarrow \text{V}^{\text{III}}$), with simultaneous formation of a new siloxide ligand at the surface of the assembly. In our approximation, this “ $\text{V}-\text{OSiMe}_3$ ” moiety

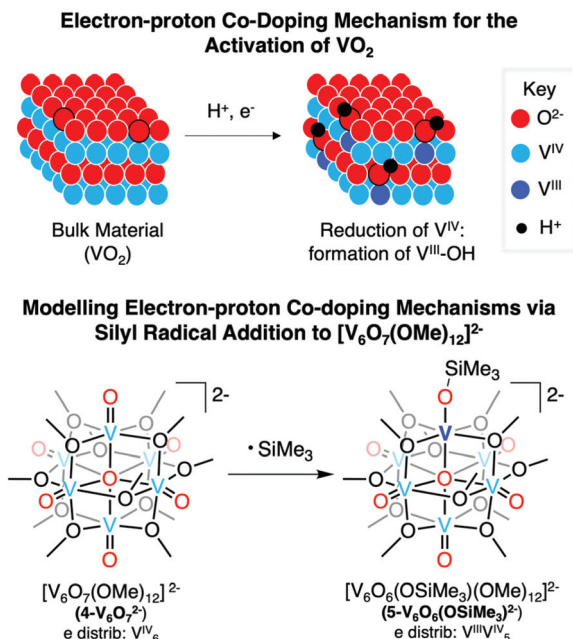


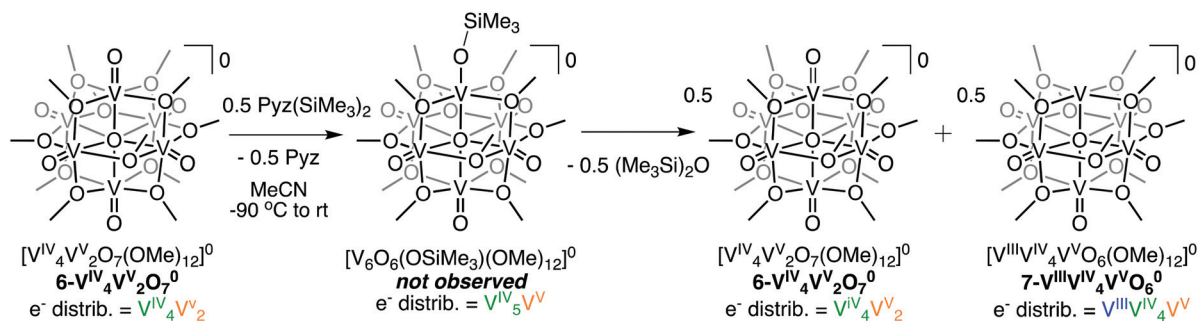
Fig. 4 Analogies between proton–electron co-doping mechanisms reported for VO_2 ^{52,53} and silyl radical transfer to the surface of $4\text{-V}_6^{\text{IV}}\text{O}_7^{2-}$.

can be correlated to the reduced “ $\text{V}-\text{OH}$ ” substituents formed in proton–electron co-doping processes described for the bulk material. One noticeable difference in the reactivity of the cluster in comparison to that of bulk VO_2 is the fact that the relative sizes of our cluster compound and $\cdot\text{SiMe}_3$ prohibits intercalation of a trimethylsilylium ion within the Lindqvist core. While limiting the direct correlations of our molecular model to the physicochemical behaviour described for the bulk material, the reactivity of $4\text{-V}_6^{\text{IV}}\text{O}_7^{2-}$ with $\cdot\text{SiMe}_3$ presents intriguing opportunities to study surface localized cation-coupled electron transfer processes (e.g. proton-coupled electron transfer) for the material that may have relevance to improved efficiency in catalysis. Ongoing investigations in our laboratory are focused on these types of reactivity.

Reactivity of $[\text{V}_5^{\text{IV}}\text{V}^{\text{V}}\text{O}_7(\text{OMe})_{12}]^0$ with Mashima's reagent

To probe the chemistry of Mashima's reagent with high-valent derivatives of the polyoxovanadate-alkoxide cluster, we next investigated the reactivity of the mixed-valent polyoxovanadate-alkoxide cluster, $[\text{V}_4^{\text{IV}}\text{V}^{\text{V}}\text{O}_7(\text{OMe})_{12}]^0$ (ox. state distrib. = $\text{V}_4^{\text{IV}}\text{V}_2^{\text{V}}$; $6\text{-V}_4^{\text{IV}}\text{V}_2^{\text{V}}\text{O}_7^0$) with $\text{Pyz}(\text{SiMe}_3)_2$ (Scheme 3). Following addition of 0.5 equiv. of $\text{Pyz}(\text{SiMe}_3)_2$ to $6\text{-V}_4^{\text{IV}}\text{V}_2^{\text{V}}\text{O}_7^0$ analysis of the crude reaction mixture by ^1H NMR spectroscopy revealed formation of a 1 : 1 mixture of the starting material, $6\text{-V}_4^{\text{IV}}\text{V}_2^{\text{V}}\text{O}_7^0$, and the previously reported neutral, oxygen-deficient polyoxovanadate-alkoxide cluster, $[\text{V}_4^{\text{III}}\text{V}_4^{\text{IV}}\text{V}^{\text{V}}\text{O}_6(\text{OMe})_{12}]^0$ ($7\text{-V}_4^{\text{III}}\text{V}_4^{\text{IV}}\text{V}^{\text{V}}\text{O}_6^0$) (Fig. 5 and Fig. S9†).⁵¹

Initially, we hypothesized that the formation of only half an equiv. of the oxygen deficient assembly was justified as follows: reductive silylation of the $\text{V}=\text{O}_t$ bond in the high



Scheme 3 Reactivity of $6\text{-V}_4\text{V}_2\text{O}_7^0$ with $\text{Pyz}(\text{SiMe}_3)_2$.

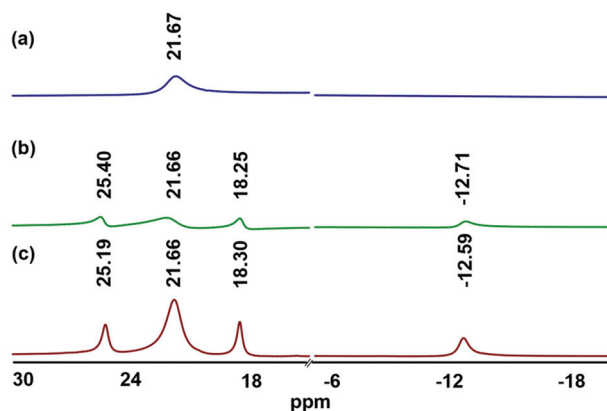


Fig. 5 ^1H -NMR (500 MHz, CD_3CN , 21°C) spectrum of (a) $6\text{-V}_4\text{V}_2\text{O}_7^0$, (b) the crude reaction mixture following the addition of 0.5 equiv. of $\text{Pyz}(\text{SiMe}_3)_2$ to $6\text{-V}_4\text{V}_2\text{O}_7^0$ in acetonitrile and (c) oxidation of $3\text{-V}_6\text{O}_6\text{OSiMe}_3^{1-}$ with AgOTf in dichloromethane. Resonances located at 25.4, 18.3, -12.7 ppm correspond to $7\text{-V}^{\text{III}}\text{V}_4\text{VVO}_6^0$ and the signal at 21.7 corresponds to $6\text{-V}_4\text{V}_2\text{O}_7^0$.

valent polyoxovanadate-alkoxide cluster is the rate determining step of the reaction. Following formation of the siloxide-functionalized polyoxovanadate-alkoxide cluster, $[\text{V}_6\text{O}_6(\text{OSiMe}_3)(\text{OMe})_{12}]^0$, preferential reactivity of Mashima's reagent with $[\text{V}_6\text{O}_6(\text{OSiMe}_3)(\text{OMe})_{12}]^0$ over the fully oxygenated species, $6\text{-V}_4\text{V}_2\text{O}_7^0$ occurs. The selective reactivity of the siloxide functionalized assembly would translate to the formation of only $\frac{1}{2}$ equiv. of $7\text{-V}^{\text{III}}\text{V}_4\text{VVO}_6^0$. To probe this hypothesis, we added a full equiv. of $\text{Pyz}(\text{SiMe}_3)_2$ to $6\text{-V}_4\text{V}_2\text{O}_7^0$, theorizing that these reaction conditions would yield complete conversion to the oxygen deficient assembly as noted in the case of $1\text{-V}_5\text{VVO}_7^{1-}$ (*vide supra*). However, analysis of the product mixture by ^1H NMR spectroscopy revealed, yet again, incomplete conversion to $7\text{-V}^{\text{III}}\text{V}_4\text{VVO}_6^0$ (Fig. S10†).

An alternative explanation for the product distribution observed upon addition of 0.5 equiv. of $\text{Pyz}(\text{SiMe}_3)_2$ to $6\text{-V}_4\text{V}_2\text{O}_7^0$ invokes formation of $[\text{V}_6\text{O}_6(\text{OSiMe}_3)(\text{OMe})_{12}]^0$, followed by rapid disproportionation of the neutral, siloxide functionalized cluster to generate $6\text{-V}_4\text{V}_2\text{O}_7^0$ and $7\text{-V}^{\text{III}}\text{V}_4\text{VVO}_6^0$. This mechanism resembles that proposed in a recent report from our research group describing proton-induced oxygen

atom vacancy formation in polyoxovanadate-ethoxide clusters.⁵⁶

In that work, we describe a proposed mechanism of O-atom vacancy formation proceeding through protonation of a terminal oxido ligand at the cluster surface, forming the transient hydroxide functionalized species, $[\text{V}_6\text{O}_6(\text{OH})(\text{OEt})_{12}]^{1-}$. Disproportionation the unstable species through purported proton coupled electron transfer results in the equimolar formation of $[\text{V}_5^{\text{IV}}\text{VVO}_7(\text{OEt})_{12}]^{1-}$ and $[\text{V}^{\text{III}}\text{V}_5\text{VVO}_6(\text{OEt})_{12}]^{1-}$. Similarly, here we can invoke silyl radical transfer to a surface vanadyl moiety, in analogy to the reactivity of $1\text{-V}_5\text{VVO}_7^{1-}$ and $4\text{-V}_6\text{O}_7^{2-}$ with 0.5 equiv. of $\text{Pyz}(\text{SiMe}_3)_2$. The siloxide moiety in $[\text{V}_6\text{O}_6(\text{OSiMe}_3)(\text{OMe})_{12}]^0$ is unstable in this oxidation state of the cluster, resulting in rapid disproportionation to generate a 1:1 ratio of $6\text{-V}_4\text{V}_2\text{O}_7^0$ and $7\text{-V}^{\text{III}}\text{V}_4\text{VVO}_6^0$ through silyl coupled electron transfer.

To further support our proposed justification for the formation of the observed mixture of products as a result of disproportionation of $[\text{V}_6\text{O}_6(\text{OSiMe}_3)(\text{OMe})_{12}]^0$, we attempted an alternative pathway to transiently access the neutral silylated species. Given the successful isolation of $3\text{-V}_6\text{O}_6(\text{OSiMe}_3)^{1-}$, we theorized that exposure of this compound to an oxidant would result in generation of the purported $[\text{V}_6\text{O}_6(\text{OSiMe}_3)(\text{OMe})_{12}]^0$ species, which would subsequently disproportionate to yield a 1:1 ratio of $6\text{-V}_4\text{V}_2\text{O}_7^0$ and $7\text{-V}^{\text{III}}\text{V}_4\text{VVO}_6^0$ (Scheme 3). Indeed, oxidation of $3\text{-V}_6\text{O}_6\text{OSiMe}_3^{1-}$ with AgOTf ($E_{1/2} = +0.65 \text{ V}$ vs. $\text{Fc}^{+/0}$ in dichloromethane⁵⁷) results in formation of equimolar amounts of $6\text{-V}_4\text{V}_2\text{O}_7^0$ and $7\text{-V}^{\text{III}}\text{V}_4\text{VVO}_6^0$ (Fig. 5c and Fig. S11†).

Conclusion

Here, we present a new route for oxygen atom defect formation at the surface of polyoxovanadate-alkoxide clusters. Addition of an equiv. of Mashima's reagent to $1\text{-V}_4\text{VVO}_7^{1-}$ results in the formation of the previously reported oxygen-deficient vanadium oxide assembly, $2\text{-V}^{\text{III}}\text{V}_5\text{VO}_6^{1-}$. Atomistic insight into the mechanism of defect formation at the polyoxovanadate-alkoxide cluster is offered through substoichiometric experiments, offering, for the first time, evidence for the formation of a siloxide-functionalized metal ion as an intermediate in oxygen-atom vacancy formation *via* reductive silylation.

Additional studies present discrepancies in the outcome of reductive silylation reactions as a function of the oxidation state of the cluster (e.g. $[\text{V}_6\text{O}_7(\text{OMe})_{12}]^n$; $n = 2-, 1-, 0$). While reactivity of the polyoxovanadate-alkoxide with $\text{Pyz}(\text{SiMe}_3)_2$ universally proceeds through an initial transfer of a silyl radical to a single vanadyl moiety of the Lindqvist core, subsequent reactivity of the resultant vanadium siloxide species is dependent on the oxidation state distribution of remote metal centres. In its reduced form, siloxide formation at the surface of the polyoxovanadate-alkoxide cluster is the terminal step of the reaction, resulting in the isolation of the fully-reduced species, $5\text{-V}^{\text{III}}\text{V}_5^{\text{IV}}\text{O}_6(\text{OSiMe}_3)^{2-}$. However, silyl radical transfer to the neutral cluster, $6\text{-V}^{\text{IV}}\text{V}_2\text{O}_7^0$, results in the transient formation of a highly unstable silylated assembly, $[\text{V}_6\text{O}_6(\text{OSiMe}_3)(\text{OMe})_{12}]^0$, which rapidly disproportionates to generate $6\text{-V}^{\text{IV}}\text{V}_2\text{O}_7^0$ and $7\text{-V}^{\text{III}}\text{V}_4\text{V}^{\text{IV}}\text{O}_6^0$. These insights offer design criteria for materials engineering *via* reductive silylation: attention must be paid to the oxidation state of the starting material in selecting reagents for surface activation of reducible metal oxides.

Experimental

All manipulations were carried out in the absence of water and oxygen using standard Schlenk techniques, or in a UniLab MBraun inert atmosphere drybox under a dinitrogen atmosphere. All glasswares were oven dried for a minimum of 4 hours and cooled in an evacuated antechamber prior to use in the drybox. Solvents were dried and deoxygenated on a Glass Contour System (Pure Process Technology, LLC) and stored over activated 3 Å molecular sieves purchased from Fisher Scientific prior to use. $[\text{Bu}_4\text{N}][\text{V}_5^{\text{IV}}\text{V}^{\text{V}}\text{O}_7(\text{OMe})_{12}]$ ($1\text{-V}_5^{\text{IV}}\text{V}^{\text{V}}\text{O}_7^{1-}$), $[\text{Bu}_4\text{N}]_2[\text{V}_6^{\text{IV}}\text{O}_7(\text{OMe})_{12}]$ ($4\text{-V}_6^{\text{IV}}\text{O}_7^{2-}$), $[\text{V}_4^{\text{IV}}\text{V}^{\text{V}}\text{O}_7(\text{OMe})_{12}]^0$ ($6\text{-V}_4^{\text{IV}}\text{V}_2\text{O}_7^0$)³¹ and $\text{Pyz}(\text{SiMe}_3)_2$ ⁵⁸ were prepared according to published procedures.

^1H NMR spectra were recorded at 500 and 400 MHz on Bruker DPX-500 and Bruker DPX-400 MHz spectrometers locked on the signal of deuterated solvents. All chemical shifts were reported relative to the peak of residual H signal in deuterated solvents. CD_3CN and CDCl_3 were purchased from Cambridge Isotope Laboratories, degassed by three freeze-pump-thaw cycles, and stored over fully activated 3 Å molecular sieves. Infrared (FT-IR, ATR) spectra of compounds were recorded on a Shimadzu IRAffinity-1 Fourier Transform Infrared Spectrophotometer and are reported in wavenumbers (cm^{-1}). Electronic absorption measurements were recorded at room temperature in anhydrous acetonitrile in a sealed 1 cm quartz cuvette with an Agilent Cary 60 UV-Vis spectrophotometer. Mass spectrometry analyses were performed on an Advion Expression^L Compact Mass Spectrometer equipped with an electrospray probe and an ion-trap mass analyser. Direct injection analysis was employed in all cases with a sample solution in acetonitrile. Liquid chromatography-MS measurements were recorded at room temperature in Thermo LTQ Velos Ion Trap Mass Spectrometer in acetonitrile.

Synthesis of $[\text{V}^{\text{III}}\text{V}_5^{\text{IV}}\text{O}_6(\text{OMe})_{12}]^{1-}$ ($2\text{-V}^{\text{III}}\text{V}_5^{\text{IV}}\text{O}_6^{1-}$) *via* reductive silylation

In a glove box, a 20 mL scintillation vial was charged with $[\text{Bu}_4\text{N}][\text{V}_6\text{O}_7(\text{OMe})_{12}]$ ($1\text{-V}_5^{\text{IV}}\text{V}^{\text{V}}\text{O}_7^{1-}$) (0.052 g, 0.050 mmol) and 4 mL dichloromethane. $\text{Pyz}(\text{SiMe}_3)_2$ (0.012 g, 0.056 mmol) was dissolved in 2 mL dichloromethane in a separate 20 mL scintillation vial. Both solutions were frozen in a liquid nitrogen cold well. The frozen solutions were taken out of the cold well and $\text{Pyz}(\text{SiMe}_3)_2$ was added drop-wise with a 1 mL syringe in five portions (0.4 mL) to the frozen slurry of $1\text{-V}_5^{\text{IV}}\text{V}^{\text{V}}\text{O}_7^{1-}$ as it thawed. The colour of the mixture changed from green to brown/red after the addition of approximately 2/3 of the $\text{Pyz}(\text{SiMe}_3)_2$ solution. After the complete addition of $\text{Pyz}(\text{SiMe}_3)_2$, the reaction was stirred for an additional 10 minutes. Residual solvent was subsequently removed under reduced pressure to give a brown solid. The crude solid was triturated with small portions of pentanes (4 mL) followed by washing with 2 mL of diethyl ether. Dichloromethane was then used to extract the product. A brown solid was obtained after dichloromethane was removed under reduced pressure. The identity of the product, $2\text{-V}^{\text{III}}\text{V}_5^{\text{IV}}\text{O}_6^{1-}$, was confirmed by ^1H NMR analysis revealing formation of the desired oxygen deficient cluster in excellent yield (94%, 0.048 g, 0.047 mmol). ^1H NMR (500 MHz, CD_3CN , 21 °C): $\delta = 25.29, 23.89, 3.08, 1.57, 1.34, 0.96, -15.51$.

Synthesis of $[\text{V}_6^{\text{IV}}\text{O}_6(\text{OSiMe}_3)(\text{OMe})_{12}]^{1-}$ ($3\text{-V}_6\text{O}_6(\text{OSiMe}_3)^{1-}$)

In a glove box, a 20 mL scintillation vial was charged with $[\text{Bu}_4\text{N}][\text{V}_4^{\text{IV}}\text{V}^{\text{V}}\text{O}_7(\text{OMe})_{12}]$ ($1\text{-V}_5^{\text{IV}}\text{V}^{\text{V}}\text{O}_7^{1-}$) (0.052 g, 0.050 mmol) and 4 mL dichloromethane. $\text{Pyz}(\text{SiMe}_3)_2$ (0.0059 mg, 0.026 mmol) was dissolved in 2 mL dichloromethane in a separate 20 mL scintillation vial. Both solutions were frozen in a liquid nitrogen cold well. The frozen solutions were taken out of the cold well and $\text{Pyz}(\text{SiMe}_3)_2$ was added drop-wise with a glass pipette in three portions to the frozen slurry of $1\text{-V}_5^{\text{IV}}\text{V}^{\text{V}}\text{O}_7^{1-}$ as it thawed. After the complete addition of $\text{Pyz}(\text{SiMe}_3)_2$, the reaction was stirred for an additional 10 minutes. Residual solvent was subsequently removed under reduced pressure to give a green solid. The crude solid was triturated with small portions of pentanes (4 mL) followed by washing with 2 mL of diethyl ether. Dichloromethane was then used to extract the product. After dichloromethane was removed under reduced pressure, the product, $3\text{-V}_6^{\text{IV}}\text{O}_6(\text{OSiMe}_3)^{1-}$ was isolated as a dark green solid in good yield (82%, 0.046 g, 0.041 mmol). ^1H NMR (500 MHz, CD_3CN , 21 °C): $\delta = 27.50$ ($\text{O}_b\text{-CH}_3$, 12 H), 24.12 ($\text{O}_b\text{-CH}_3$, 12 H), 3.06 ($[\text{N}(\text{CH}_2\text{CH}_2\text{CH}_2\text{CH}_3)_4]^{1+}$, 8 H), 1.57 ($[\text{N}(\text{CH}_2\text{CH}_2\text{CH}_2\text{CH}_3)_4]^{1+}$, 8 H), 1.34 ($[\text{N}(\text{CH}_2\text{CH}_2\text{CH}_2\text{CH}_3)_4]^{1+}$, 8 H), 0.96 ($[\text{N}(\text{CH}_2\text{CH}_2\text{CH}_2\text{CH}_3)_4]^{1+}$, 12 H), -9.79 ($\text{O}_b\text{-CH}_3$, 12 H). Elemental analysis for $\text{C}_{31}\text{H}_{81}\text{NO}_{19}\text{V}_6\text{Si}_{0.5}\text{CH}_2\text{Cl}_2$ (MW = 1148.17 g mol⁻¹) calcd (%): C, 32.95; H, 7.20; N, 1.22. Found (%): C, 32.99; H, 7.21; N 0.89. FT-IR (ATR, cm^{-1}): 1462, 1446, 1248, 1044 ($\text{O}_b\text{-CH}_3$), 955 (V=O), 874, 840. UV-Vis: (CH_3CN): 1000 nm ($\epsilon = 505 \text{ M}^{-1} \text{ cm}^{-1}$).

Synthesis of $[V^{III}V_5^{IV}O_6(OSiMe_3)(OMe)_{12}]^{2-}$ ($5-V^{III}V_5^{IV}O_6(OSiMe_3)^{2-}$)

In a glove box, a 20 mL scintillation vial was charged with $[^nBu_4N]_2[V_6^{IV}O_7(OMe)_{12}]$ ($4-V_6^{IV}O_7^{2-}$) (0.060 g, 0.048 mmol) and 4 mL acetonitrile. $Pyz(SiMe_3)_2$ (0.006 g, 0.027 mmol) was dissolved in 2 mL acetonitrile in a separate 20 mL scintillation vial. Both solutions were frozen in a liquid nitrogen cold well. The frozen solutions were removed from the cold well and left to thaw; $Pyz(SiMe_3)_2$ was added drop-wise with a glass pipette in three portions to the frozen slurry of $4-V_6^{IV}O_7^{2-}$. The reaction mixture was stirred for an additional 10 minutes. Residual solvent was subsequently removed under reduced pressure to give a blue-green solid. The crude solid was triturated with small portions of pentanes (4 mL) followed by washing with 2 mL of diethyl ether. Tetrahydrofuran was then used to extract the product. Following removal of the residual solvent under vacuum, the product, $5-V^{III}V_5^{IV}O_6(OSiMe_3)^{2-}$, was isolated as a blue-green solid in low yield (4%, 0.003 g, 0.002 mmol). 1H NMR (500 MHz, CD_3CN , 21 °C): δ = 24.77 (O_b-CH_3 , 12 H), 22.75 (O_b-CH_3 , 12 H), 3.07 ($[N(CH_2CH_2CH_2CH_3)_4]^{1+}$, 8 H), 1.58 ($[N(CH_2CH_2CH_2CH_3)_4]^{1+}$, 8 H), 1.33 ($[N(CH_2CH_2CH_2CH_3)_4]^{1+}$, 8 H), 0.96 ($[N(CH_2CH_2CH_2CH_3)_4]^{1+}$, 12 H), -8.41 (O_b-CH_3 , 12 H). Elemental analysis for $C_{47}H_{117}N_2O_{19}V_6Si \cdot CH_2Cl_2$ (MW = 1348.17 g mol $^{-1}$) calcd (%): C, 40.23; H, 8.37; N, 1.95. Found (%): C, 40.47; H, 8.07; N 1.82. FT-IR (ATR, cm $^{-1}$): 1468, 1416, 1233, 1063 (O_b-CH_3), 939 ($V=O$), 818, 737. UV-Vis: (CH_3CN): 1000 nm (ϵ = 126 M $^{-1}$ cm $^{-1}$), 626 nm (ϵ = 39 M $^{-1}$ cm $^{-1}$).

Reaction of $6-V_4^{IV}V_2^{IV}O_7^0$ with 0.5 equiv. of $Pyz(SiMe_3)_2$

In a glove box, a 20 mL scintillation vial was charged with $[V_4^{IV}V_2^{IV}O_7(OMe)_{12}]$ $6-V_4^{IV}V_2^{IV}O_7^0$ (0.052 g, 0.066 mmol) and 4 mL acetonitrile. In a separate vial, $Pyz(SiMe_3)_2$ (0.0082 g, 0.036 mmol) was dissolved in 2 mL acetonitrile. Both solutions were frozen in a liquid nitrogen cold well prior to adding the $Pyz(SiMe_3)_2$ solution to the polyoxovanadate-alkoxide cluster, drop-wise while the solutions thawed. After the complete addition of $Pyz(SiMe_3)_2$, the reaction was stirred for an additional 10 minutes. Residual solvent was subsequently removed under reduced pressure to give a brownish green solid. 1H -NMR analysis of the solid product revealed the formation of equimolar amounts of $6-V_4^{IV}V_2^{IV}O_7^0$ and $7-V^{III}V_4^{IV}V^{IV}O_6^0$, as determined by integration.

Reaction of $6-V_4^{IV}V_2^{IV}O_7^0$ with 1 equiv. of $Pyz(SiMe_3)_2$

In a glove box, a 20 mL scintillation vial was charged with $6-V_4^{IV}V_2^{IV}O_7^0$ (0.052 g, 0.066 mmol) and 4 mL acetonitrile. $Pyz(SiMe_3)_2$ (0.0163 g, 0.072 mmol) was dissolved in 2 mL acetonitrile in a separate 20 mL scintillation vial. Both solutions were frozen in a liquid nitrogen cold well. The frozen solutions were taken out of the cold well and $Pyz(SiMe_3)_2$ was added drop-wise with a glass pipette in three portions to the frozen slurry of $6-V_4^{IV}V_2^{IV}O_7^0$ as it thawed. After the complete addition of $Pyz(SiMe_3)_2$, the reaction was stirred for an additional 10 minutes. Residual solvent was subsequently removed under reduced pressure to give a brownish green solid. 1H -NMR ana-

lysis of the green solid confirmed formation of a mixture of products, namely $6-V_4^{IV}V_2^{IV}O_7^0$ and $7-V^{III}V_4^{IV}V^{IV}O_6^0$.

Oxidation of $3-V_6^{IV}O_6(OSiMe_3)^{1-}$

In a glove box, a 20 mL scintillation vial was charged with $3-V_6^{IV}O_6(OSiMe_3)^{1-}$ (0.039 g, 0.035 mmol) and 4 mL dichloromethane. $AgOTf$ (0.0107 mg, 0.042 mmol) was dissolved in 2 mL dichloromethane in a separate 20 mL scintillation vial. Both solutions were frozen in a liquid nitrogen cold well. The frozen solutions were removed from the cold well; the solution containing $AgOTf$ was added drop-wise to the frozen slurry of $3-V_6^{IV}O_6(OSiMe_3)^{1-}$ as it thawed. Following the complete addition of $AgOTf$, the reaction was stirred for an additional 10 minutes. Residual solvent was removed under reduced pressure, resulting in the isolation of a brown-green solid. 1H -NMR analysis of the crude product revealed the formation of equimolar amounts of $6-V_4^{IV}V_2^{IV}O_7^0$ and $7-V^{III}V_4^{IV}V^{IV}O_6^0$.

Conflicts of interest

There are no conflicts to declare.

Acknowledgements

This research was funded by the National Science Foundation through grant CHE-1653195. E. M. M. is a recipient of a Cottrell Scholar Award from the Research Corporation for Science Advancement, and a Sloan Research Fellowship from the Alfred P. Sloan Foundation, which have provided additional resources to support this research. The authors would like to acknowledge Eric Schreiber for helpful conversation and advise during the construction of this manuscript.

References

- 1 C. Yuan, H. B. Wu, Y. Xie and X. W. Lou, Mixed Transition-Metal Oxides: Design, Synthesis, and Energy-Related Applications, *Angew. Chem., Int. Ed.*, 2014, **53**, 1488–1504.
- 2 X. Yu, T. J. Marks and A. Facchetti, Metal oxides for optoelectronic applications, *Nat. Mater.*, 2016, **15**, 383–396.
- 3 X. Xia, Y. Zhang, D. Chao, C. Guan, Y. Zhang, L. Li, X. Ge, I. M. Bacho, J. Tu and H. J. Fan, Solution synthesis of metal oxides for electrochemical energy storage applications, *Nanoscale*, 2014, **6**, 5008–5048.
- 4 E. W. McFarland and H. Metiu, Catalysis by Doped Oxides, *Chem. Rev.*, 2013, **113**, 4391–4427.
- 5 A. Ruiz Puigdollers, P. Schlexer, S. Tosoni and G. Pacchioni, Increasing Oxide Reducibility: The Role of Metal/Oxide Interfaces in the Formation of Oxygen Vacancies, *ACS Catal.*, 2017, **7**, 6493–6513.
- 6 J. Jia, C. Qian, Y. Dong, Y. F. Li, H. Wang, M. Ghoussoub, K. T. Butler, A. Walsh and G. A. Ozin, Heterogeneous catalytic hydrogenation of CO_2 by metal oxides: defect engin-

- eering – perfecting imperfection, *Chem. Soc. Rev.*, 2017, **46**, 4631–4644.
- 7 P. L. Gai-Boyes, Defects in Oxide Catalysts: Fundamental Studies of Catalysis in Action, *Catal. Rev.*, 1992, **34**, 1–54.
 - 8 M. Ek, Q. M. Ramasse, L. Arnarson, P. Georg Moses and S. Helveg, Visualizing atomic-scale redox dynamics in vanadium oxide-based catalysts, *Nat. Commun.*, 2017, **8**, 305.
 - 9 U. Diebold, The surface science of titanium dioxide, *Surf. Sci. Rep.*, 2003, **48**, 53–229.
 - 10 L. Artiglia, S. Agnoli and G. Granozzi, Vanadium oxide nanostructures on another oxide: The viewpoint from model catalysts studies, *Coord. Chem. Rev.*, 2015, **301–302**, 106–122.
 - 11 P. Mars and D. W. van Krevelen, Oxidations carried out by means of vanadium oxide catalysts, *Chem. Eng. Sci.*, 1954, **3**, 41–59.
 - 12 C. Doornkamp and V. Ponc, The universal character of the Mars and Van Krevelen mechanism, *J. Mol. Catal. A: Chem.*, 2000, **162**, 19–32.
 - 13 D. R. Mullins, The surface chemistry of cerium oxide, *Surf. Sci. Rep.*, 2015, **70**, 42–85.
 - 14 H. Over, Y. D. Kim, A. P. Seitsonen, S. Wendt, E. Lundgren, M. Schmid, P. Varga, A. Morgante and G. Ertl, Atomic-Scale Structure and Catalytic Reactivity of the RuO₂(110) Surface, *Science*, 2000, **287**, 1474.
 - 15 S. Surnev, M. G. Ramsey and F. P. Netzer, Vanadium oxide surface studies, *Prog. Surf. Sci.*, 2003, **73**, 117–165.
 - 16 M. M. Montemore, M. A. van Spronsen, R. J. Madix and C. M. Friend, O₂ Activation by Metal Surfaces: Implications for Bonding and Reactivity on Heterogeneous Catalysts, *Chem. Rev.*, 2018, **118**, 2816–2862.
 - 17 J. Jupille and G. Thornton, in *Defects at Oxide Surfaces*, Springer, Heidelberg, Germany, 2015.
 - 18 M. V. Ganduglia-Pirovano, A. Hofmann and J. Sauer, Oxygen vacancies in transition metal and rare earth oxides: Current state of understanding and remaining challenges, *Surf. Sci. Rep.*, 2007, **62**, 219–270.
 - 19 H. Tsurugi and K. Mashima, Salt-Free Reduction of Transition Metal Complexes by Bis(trimethylsilyl)cyclohexadiene, -dihydropyrazine, and -4,4'-bipyridinylidene Derivatives, *Acc. Chem. Res.*, 2019, **52**, 769–779.
 - 20 T. Saito, H. Nishiyama, H. Tanahashi, K. Kawakita, H. Tsurugi and K. Mashima, 1,4-Bis(trimethylsilyl)-1,4-diaza-2,5-cyclohexadienes as Strong Salt-Free Reductants for Generating Low-Valent Early Transition Metals with Electron-Donating Ligands, *J. Am. Chem. Soc.*, 2014, **136**, 5161–5170.
 - 21 V. Mougél, K.-W. Chan, G. Siddiqi, K. Kawakita, H. Nagae, H. Tsurugi, K. Mashima, O. Safonova and C. Copéret, Low Temperature Activation of Supported Metathesis Catalysts by Organosilicon Reducing Agents, *ACS Cent. Sci.*, 2016, **2**, 569–576.
 - 22 K. Yamamoto, K. W. Chan, V. Mougél, H. Nagae, H. Tsurugi, O. V. Safonova, K. Mashima and C. Copéret, Silica-supported isolated molybdenum di-oxo species: formation and activation with organosilicon agent for olefin metathesis, *Chem. Commun.*, 2018, **54**, 3989–3992.
 - 23 X. López, J. J. Carbó, C. Bo and J. M. Poblet, Structure, properties and reactivity of polyoxometalates: a theoretical perspective, *Chem. Soc. Rev.*, 2012, **41**, 7537–7571.
 - 24 D.-L. Long, E. Burkholder and L. Cronin, Polyoxometalate clusters, nanostructures and materials: From self assembly to designer materials and devices, *Chem. Soc. Rev.*, 2007, **36**, 105–121.
 - 25 L. Cronin and A. Müller, From serendipity to design of polyoxometalates at the nanoscale, aesthetic beauty and applications, *Chem. Soc. Rev.*, 2012, **41**, 7333–7334.
 - 26 A. M. Khenkin, L. Weiner, Y. Wang and R. Neumann, Electron and Oxygen Transfer in Polyoxometalate, H₅PV₂Mo₁₀O₄₀, Catalyzed Oxidation of Aromatic and Alkyl Aromatic Compounds: Evidence for Aerobic Mars–van Krevelen-Type Reactions in the Liquid Homogeneous Phase, *J. Am. Chem. Soc.*, 2001, **123**, 8531–8542.
 - 27 I. Efremenko and R. Neumann, Computational Insight into the Initial Steps of the Mars–van Krevelen Mechanism: Electron Transfer and Surface Defects in the Reduction of Polyoxometalates, *J. Am. Chem. Soc.*, 2012, **134**, 20669–20680.
 - 28 A. M. Khenkin, G. Leitius and R. Neumann, Electron Transfer–Oxygen Transfer Oxygenation of Sulfides Catalyzed by the H₅PV₂Mo₁₀O₄₀ Polyoxometalate, *J. Am. Chem. Soc.*, 2010, **132**, 11446–11448.
 - 29 B. E. Petel and E. M. Matson, Oxygen-atom vacancy formation and reactivity in polyoxovanadate clusters, *Chem. Commun.*, 2020, **56**, 13477–13490.
 - 30 J. Spandl, C. Daniel, I. Brüdgam and H. Hartl, Synthesis and Structural Characterization of Redox-Active Dodecamethoxoheptaooxohexavanadium Clusters, *Angew. Chem., Int. Ed.*, 2003, **42**, 1163–1166.
 - 31 C. Daniel and H. Hartl, Neutral and Cationic V^{IV}/V^V Mixed-Valence Alkoxo-polyoxovanadium Clusters [V₆O₇(OR)₁₂]ⁿ⁺ (R = –CH₃, –C₂H₅): Structural, Cyclovoltammetric and IR-Spectroscopic Investigations on Mixed Valency in a Hexanuclear Core, *J. Am. Chem. Soc.*, 2005, **127**, 13978–13987.
 - 32 C. Daniel and H. Hartl, A Mixed-Valence V^{IV}/V^V Alkoxo-polyoxovanadium Cluster Series [V₆O₈(OCH₃)₁₁]^{n+/–}: Exploring the Influence of a μ-Oxo Ligand in a Spin Frustrated Structure, *J. Am. Chem. Soc.*, 2009, **131**, 5101–5114.
 - 33 L. E. VanGelder, A. M. Kosswattaarachchi, P. L. Forrestel, T. R. Cook and E. M. Matson, Polyoxovanadate-alkoxide clusters as multi-electron charge carriers for symmetric non-aqueous redox flow batteries, *Chem. Sci.*, 2018, **9**, 1692–1699.
 - 34 M. B. Robin and P. Day, in *Advances in Inorganic Chemistry and Radiochemistry*, ed. H. J. Emeléus and A. G. Sharpe, Academic Press, 1968, vol. 10, pp. 247–422.
 - 35 B. E. Petel and E. M. Matson, Conversion of NO_x^{1–} (x = 2, 3) to NO using an oxygen-deficient polyoxovanadate-alkoxide cluster, *Chem. Commun.*, 2020, **56**, 555–558.
 - 36 B. E. Petel, R. L. Meyer, W. W. Brennessel and E. M. Matson, Oxygen atom transfer with organofunctiona-

- lized polyoxovanadium clusters: O-atom vacancy formation with tertiary phosphanes and deoxygenation of styrene oxide, *Chem. Sci.*, 2019, **10**, 8035–8045.
- 37 B. E. Petel and E. M. Matson, Physicochemical Factors That Influence the Deoxygenation of Oxyanions in Atomically Precise, Oxygen-Deficient Vanadium Oxide Assemblies, *Inorg. Chem.*, 2020, **60**, 6855–6864.
 - 38 B. E. Petel, W. W. Brennessel and E. M. Matson, Oxygen-Atom Vacancy Formation at Polyoxovanadate Clusters: Homogeneous Models for Reducible Metal Oxides, *J. Am. Chem. Soc.*, 2018, **140**, 8424–8428.
 - 39 S. Chakraborty, E. Schreiber, K. R. Sanchez-Lievanos, M. Tariq, W. W. Brennessel, K. E. Knowles and E. M. Matson, Modelling local structural and electronic consequences of proton and hydrogen-atom uptake in VO₂ with polyoxovanadate clusters, *Chem. Sci.*, 2021, DOI: 10.1039/D1SC02809J.
 - 40 S. Uchida, T. Okunaga, Y. Harada, S. Magira, Y. Noda, T. Mizuno and T. Tachikawa, Rapid formation of small mixed-valence luminescent silver clusters via cation-coupled electron-transfer in a redox-active porous ionic crystal based on dodecamolybdophosphate, *Nanoscale*, 2019, **11**, 5460–5466.
 - 41 R. Kawahara, S. Uchida and N. Mizuno, Redox-Induced Reversible Uptake–Release of Cations in Porous Ionic Crystals Based on Polyoxometalate: Cooperative Migration of Electrons with Alkali Metal Ions, *Chem. Mater.*, 2015, **27**, 2092–2099.
 - 42 S. Uchida, Frontiers and progress in cation-uptake and exchange chemistry of polyoxometalate-based compounds, *Chem. Sci.*, 2019, **10**, 7670–7679.
 - 43 E. Schreiber, N. A. Hartley, W. W. Brennessel, T. R. Cook, J. R. McKone and E. M. Matson, An Organofunctionalized Polyoxovanadium Cluster as a Molecular Model of Interfacial Pseudocapacitance, *ACS Appl. Energy Mater.*, 2019, **2**, 8985–8993.
 - 44 W. H. Knoth, Derivatives of heteropolyanions. 1. Organic derivatives of W₁₂SiO₄₀^{4–}, W₁₂PO₄₀^{3–}, and Mo₁₂SiO₄₀^{4–}, *J. Am. Chem. Soc.*, 1979, **101**, 759–760.
 - 45 A. Proust, R. Thouvenot and P. Gouzerh, Functionalization of polyoxometalates: towards advanced applications in catalysis and materials science, *Chem. Commun.*, 2008, 1837–1852.
 - 46 I. Bar-Nahum and R. Neumann, Synthesis, characterization and catalytic activity of a Wilkinson's type metal-organic-polyoxometalate hybrid compound, *Chem. Commun.*, 2003, 2690–2691.
 - 47 I. Bar-Nahum, H. Cohen and R. Neumann, Organometallic–Polyoxometalate Hybrid Compounds: Metallosalen Compounds Modified by Keggin Type Polyoxometalates, *Inorg. Chem.*, 2003, **42**, 3677–3684.
 - 48 F. Odobel, M. Séverac, Y. Pellegrin, E. Blart, C. Fosse, C. Cannizzo, C. R. Mayer, K. J. Elliott and A. Harriman, Coupled Sensitizer–Catalyst Dyads: Electron-Transfer Reactions in a Perylene–Polyoxometalate Conjugate, *Chem. – Eur. J.*, 2009, **15**, 3130–3138.
 - 49 V. W. Day, W. G. Klemperer and C. Schwartz, Synthesis, characterization, and interconversion of the niobotungstic acid Nb₂W₄O₁₉H₃[–] and its anhydride and alkyl/silyl esters, *J. Am. Chem. Soc.*, 1987, **109**, 6030–6044.
 - 50 F. Bannani, R. Thouvenot and M. Debbabi, Synthesis and Characterization of New Organosilyl Derivatives of Polyoxometalates (nBu₄N)₂[NbW₅O₁₉SiRR'₂] (R = R' = Et, iPr, OtBu, Ph; R = tBu and R' = Me) – X-ray Crystal Structure of (nBu₄N)₂[NbW₅O₁₉SiPh₃], *Eur. J. Inorg. Chem.*, 2007, 4357–4363.
 - 51 B. E. Petel, A. A. Fertig, M. L. Maiola, W. W. Brennessel and E. M. Matson, Controlling Metal-to-Oxygen Ratios via M=O Bond Cleavage in Polyoxovanadate Alkoxide Clusters, *Inorg. Chem.*, 2019, **58**, 10462–10471.
 - 52 Y. Chen, Z. Wang, S. Chen, H. Ren, L. Wang, G. Zhang, Y. Lu, J. Jiang, C. Zou and Y. Luo, Non-catalytic hydrogenation of VO₂ in acid solution, *Nat. Commun.*, 2018, **9**, 818.
 - 53 B. Li, L. Xie, Z. Wang, S. Chen, H. Ren, Y. Chen, C. Wang, G. Zhang, J. Jiang and C. Zou, Electron–Proton Co-doping-Induced Metal–Insulator Transition in VO₂ Film via Surface Self-Assembled L-Ascorbic Acid Molecules, *Angew. Chem., Int. Ed.*, 2019, **58**, 13711–13716.
 - 54 J. Chu, T. G. Carroll, G. Wu, J. Telser, R. Dobrovetsky and G. Ménard, Probing Hydrogen Atom Transfer at a Phosphorus(V) Oxide Bond Using a “Bulky Hydrogen Atom” Surrogate: Analogies to PCET, *J. Am. Chem. Soc.*, 2018, **140**, 15375–15383.
 - 55 B. E. Petel, R. L. Meyer, M. L. Maiola, W. W. Brennessel, A. M. Müller and E. M. Matson, Site-Selective Halogenation of Polyoxovanadate Clusters: Atomically Precise Models for Electronic Effects of Anion Doping in VO₂, *J. Am. Chem. Soc.*, 2020, **142**, 1049–1056.
 - 56 E. Schreiber, B. E. Petel and E. M. Matson, Acid-Induced, Oxygen-Atom Defect Formation in Reduced Polyoxovanadate-Alkoxide Clusters, *J. Am. Chem. Soc.*, 2020, **142**, 9915–9919.
 - 57 N. G. Connelly and W. E. Geiger, Chemical Redox Agents for Organometallic Chemistry, *Chem. Rev.*, 1996, **96**, 877–910.
 - 58 R. A. Sulzbach and A. F. M. Iqbal, 1,4-Bis(trimethylsilyl)-1,4-dihydropyrazine by Reductive Silylation of Pyrazine, *Angew. Chem., Int. Ed. Engl.*, 1971, **10**, 127–127.

Reductive Silylation of Polyoxovanadate Surfaces using Mashima's Reagent

Sourav Chakraborty and Ellen M. Matson*

Department of Chemistry, University of Rochester, Rochester, New York 14627, USA.

Corresponding author email: matson@chem.rochester.edu

Supporting Information Table of contents.

Fig. S1: ^1H NMR spectra of $1\text{-V}_6\text{O}_7^{1-}$ and $2\text{-V}_6\text{O}_6^{1-}$	S2
Fig. S2: LC-MS of pentane wash of the reaction of $1\text{-V}_6\text{O}_7^{1-}$ with 1 equiv $\text{Pyz}(\text{SiMe}_3)_2$	S2
Fig. S3: ^1H NMR spectrum of $2\text{-V}_6\text{O}_6^{1-}$ synthesis (crude).....	S3
Fig. S4: ^1H NMR spectrum of $3\text{-V}_6\text{O}_6(\text{OSiMe}_3)^{1-}$ synthesis.....	S3
Fig. S5: ^1H NMR spectrum of pure $3\text{-V}_6\text{O}_6(\text{OSiMe}_3)^{1-}$	S3
Fig. S6: ^1H NMR spectrum of $2\text{-V}_6\text{O}_6^{1-}$	S4
Fig. S7: LC-MS of pentane wash of the reaction of $3\text{-V}_6\text{O}_6(\text{OSiMe}_3)^{1-}$ with 0.5 equiv $\text{Pyz}(\text{SiMe}_3)_2$	S4
Fig. S8: ^1H NMR spectrum of $5\text{-V}_6\text{O}_6(\text{OSiMe}_3)^{2-}$	S5
Fig. S9: ^1H NMR spectrum of $6\text{-V}_6\text{O}_7^0$ and the crude reaction mixture following the addition of 0.5 equiv of $\text{Pyz}(\text{SiMe}_3)_2$ to $6\text{-V}_6\text{O}_7^0$	S5
Fig. S10: ^1H NMR spectrum of the crude reaction mixture following the addition of 1 equiv of $\text{Pyz}(\text{SiMe}_3)_2$ to $6\text{-V}_6\text{O}_7^0$	S6
Fig. S11: ^1H NMR spectrum of $3\text{-V}_6\text{O}_6\text{OSiMe}_3^{1-}$ oxidation with 1.0 equiv AgOTf	S6
Fig. S12: Thermal degradation of $3\text{-V}_6\text{O}_6\text{OSiMe}_3^{1-}$	S6
Fig. S13: ^1H NMR spectrum of the reaction following the addition of 0.5 equiv of $\text{Pyz}(\text{SiMe}_3)_2$ to $1\text{-V}_6\text{O}_7^{1-}$ in acetonitrile.....	S7
Fig. S14: ^1H NMR spectrum of the reaction following the addition of 0.55 equiv of $\text{Pyz}(\text{SiMe}_3)_2$ to $1\text{-V}_6\text{O}_7^{1-}$ in dichloromethane.....	S7

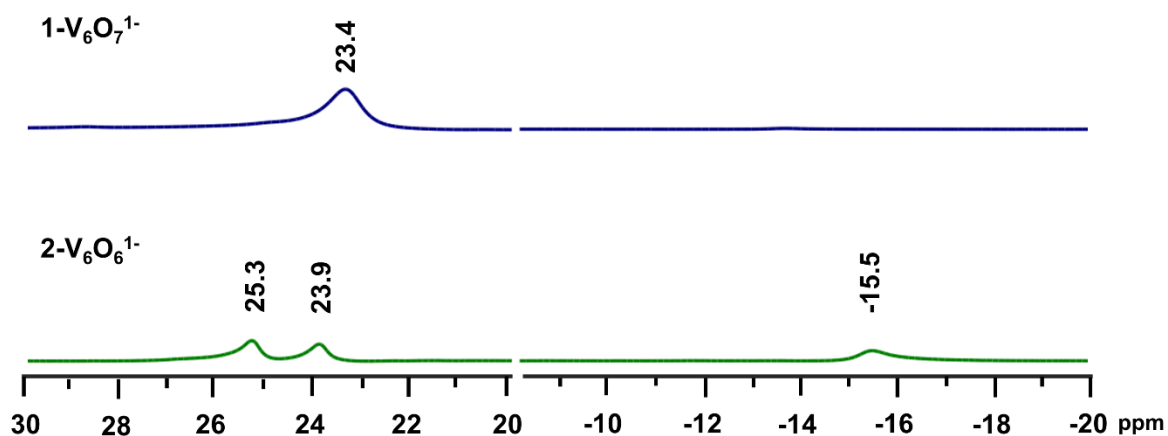


Fig. S1. ^1H NMR (500 MHz, CD_3CN , 21 $^\circ\text{C}$) spectra of $1\text{-V}_6\text{O}_7^{1-}$ and $2\text{-V}_6\text{O}_6^{1-}$.

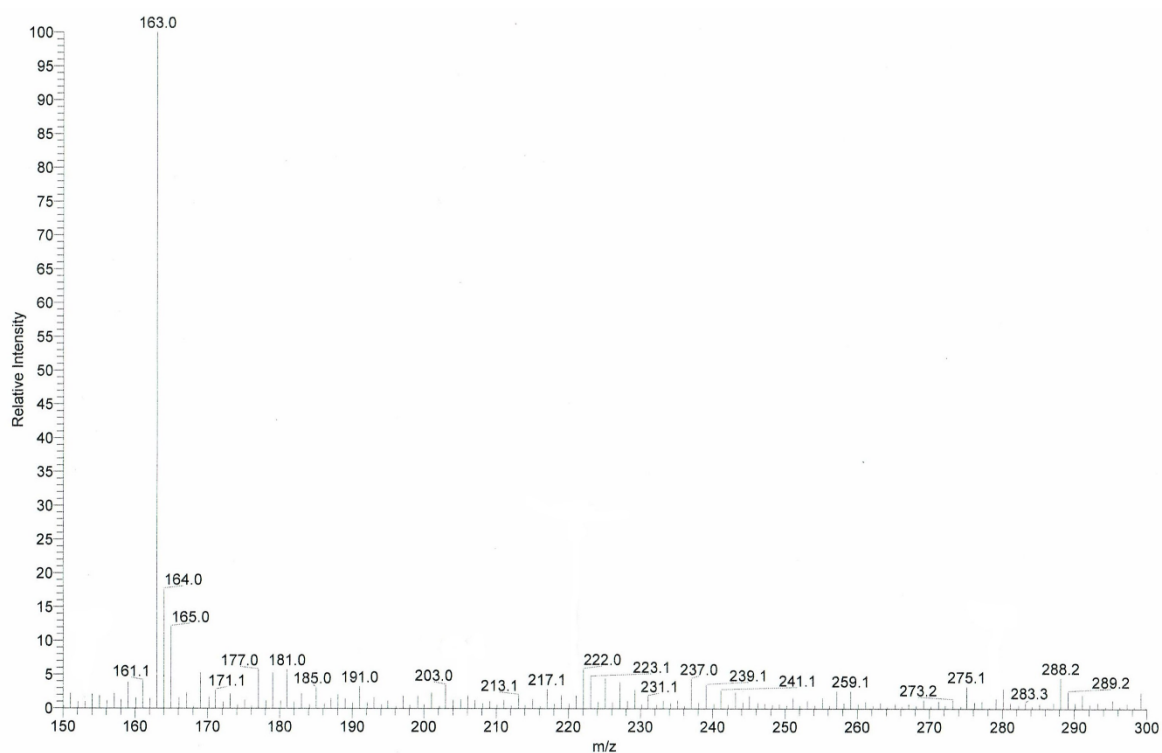


Fig. S2. LC-MS of pentane wash of the reaction of $1\text{-V}_6\text{O}_7^{1-}$ with 1 equiv $\text{Pyz}(\text{SiMe}_3)_2$ in dichloromethane. The peak at $m/z = 163$ ($\text{M}+\text{H}^+$) amu corresponds to $(\text{Me}_3\text{Si})_2\text{O}$.

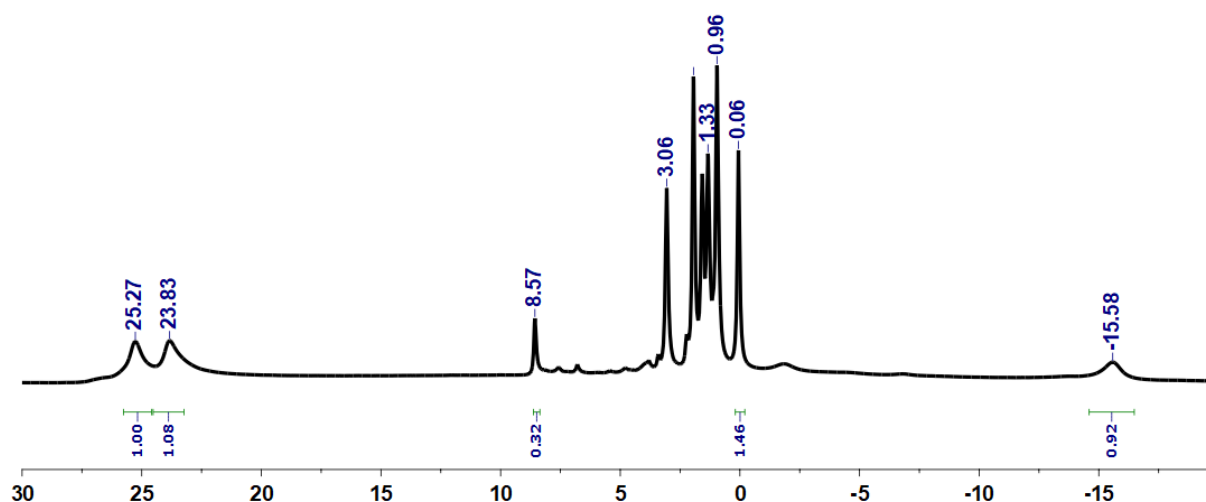


Fig. S3. ^1H NMR (500 MHz, CD_3CN , 21 $^\circ\text{C}$) spectrum of the crude reaction mixture following the addition of 1 equiv of $\text{Pyz}(\text{SiMe}_3)_2$ to $1\text{-V}_6\text{O}_7^{1-}$ in dichloromethane to form $2\text{-V}_6\text{O}_6^{1-}$. The peak integration for 36 protons of $2\text{-V}_6\text{O}_6^{1-}$ correspond to 3, *i.e.* integration for each proton is 0.083. The integration of 8.57 ppm (for pyrazine) stands for 4 protons and the integration of 0.06 ppm (TMS_2O) stands for 18 protons. This represents formation of one equivalent of pyrazine and TMS_2O .

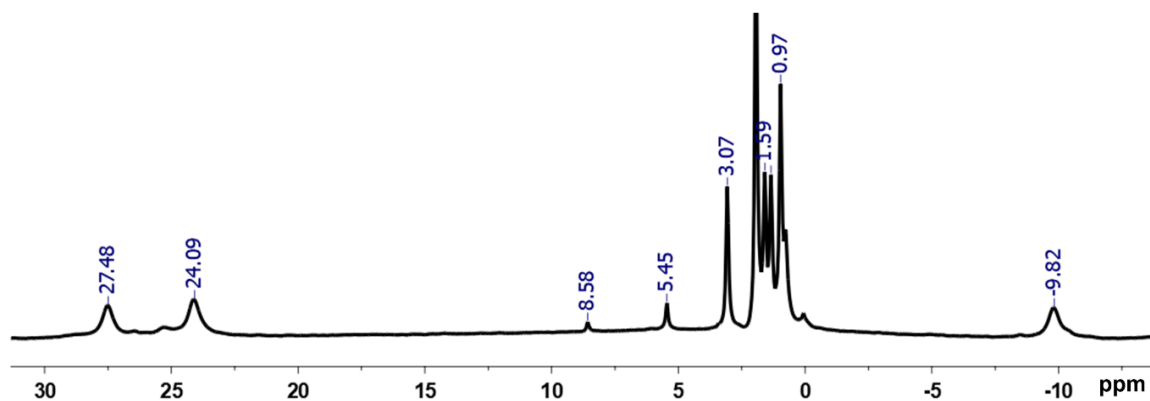


Fig. S4. ^1H NMR (500 MHz, CD_3CN , 21 $^\circ\text{C}$) spectrum of the crude reaction mixture of $3\text{-V}_6\text{O}_6(\text{OSiMe}_3)^{1-}$. The peak at 8.58 ppm (CD_3CN , 21 $^\circ\text{C}$) signifies the formation of pyrazine.

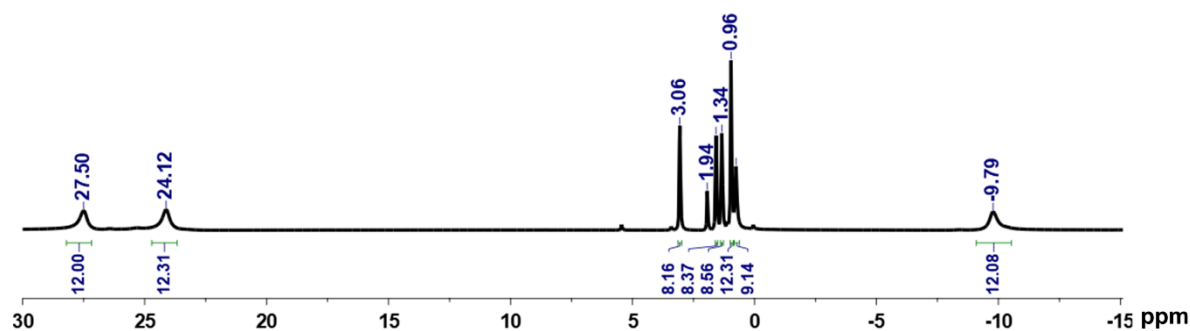


Fig. S5. ^1H NMR (500 MHz, CD_3CN , 21 $^\circ\text{C}$) spectrum of $3\text{-V}_6\text{O}_6(\text{OSiMe}_3)^{1-}$.

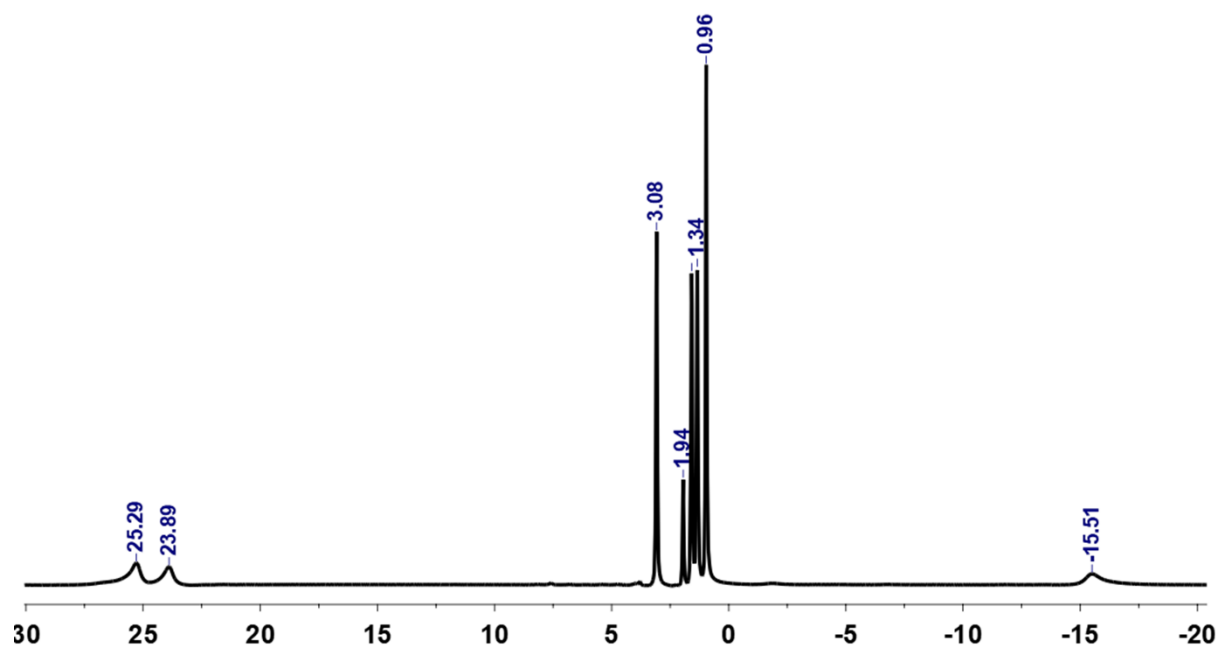


Fig. S6. ^1H NMR (500 MHz, CD_3CN , 21 $^\circ\text{C}$) spectrum of $2\text{-V}_6\text{O}_6^{1-}$ formed as a product of the reaction between $3\text{-V}_6\text{O}_6(\text{OSiMe}_3)^{1-}$ and 0.5 equiv. $\text{Pyz}(\text{SiMe}_3)_2$ in dichloromethane at low temperature.

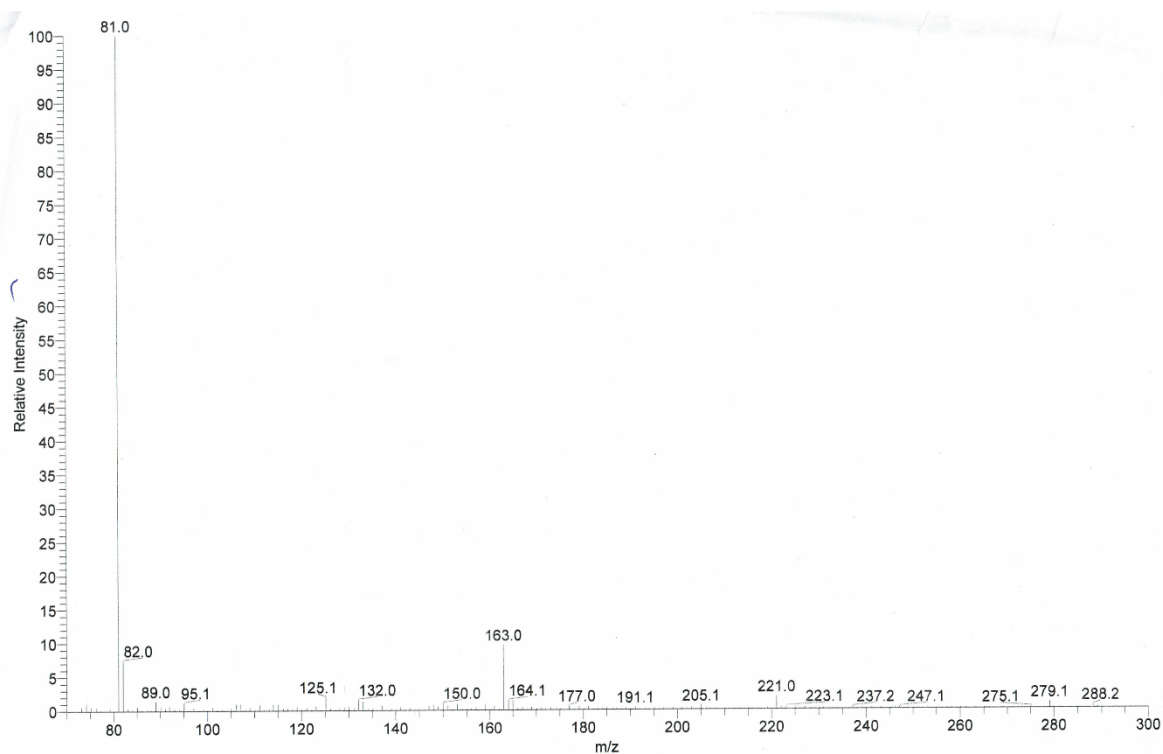


Fig. S7. LC-MS of pentane wash of the reaction of $3\text{-V}_6\text{O}_6(\text{OSiMe}_3)^{1-}$ with 0.5 eq. $\text{Pyz}(\text{SiMe}_3)_2$ in dichloromethane. The peak at $m/z = 81$ ($\text{M}+\text{H}^+$) amu and $m/z = 163$ ($\text{M}+\text{H}^+$) amu correspond to pyrazine and $(\text{Me}_3\text{Si})_2\text{O}$ respectively.

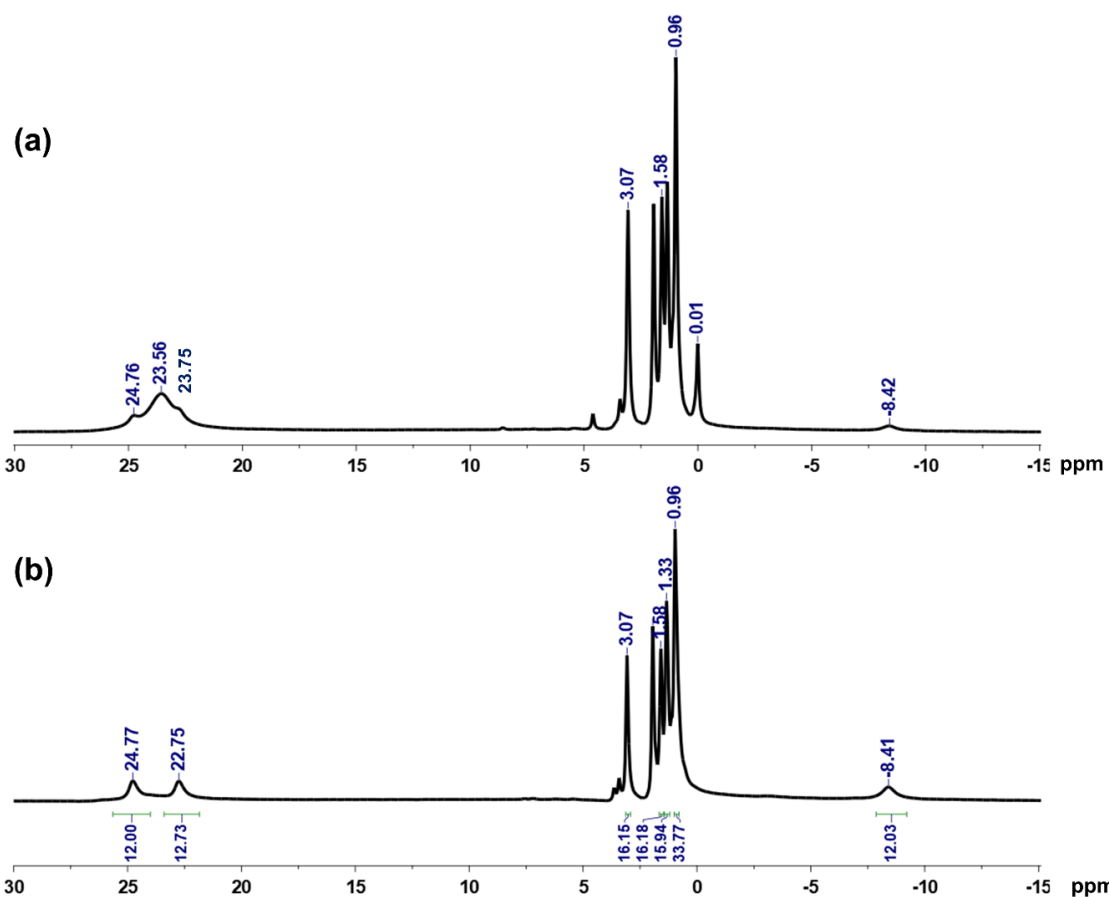


Fig. S8. ^1H NMR (500 MHz, CD_3CN , 21 $^\circ\text{C}$) spectrum of (a) the crude reaction mixture of the synthesis of $5\text{-V}_6\text{O}_6(\text{OSiMe}_3)^{2-}$, and (b) $5\text{-V}_6\text{O}_6(\text{OSiMe}_3)^{2-}$ following work-up.

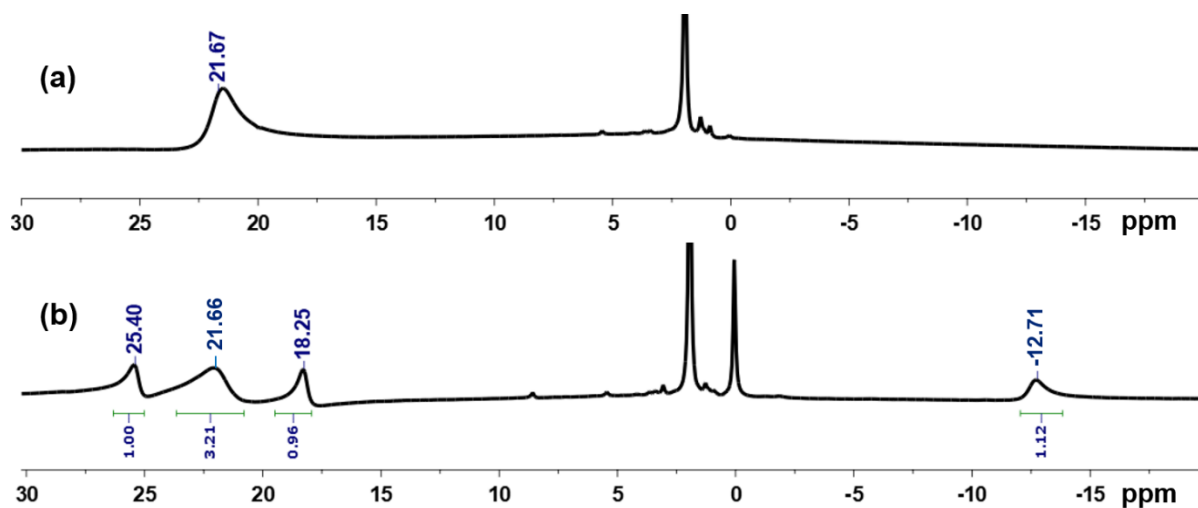


Fig. S9. ^1H NMR (500 MHz, CD_3CN , 21 $^\circ\text{C}$) spectrum of (a) $6\text{-V}_6\text{O}_7^0$, (b) the crude reaction mixture following the addition of 0.5 equiv of $\text{Pyz}(\text{SiMe}_3)_2$ to $6\text{-V}_6\text{O}_7^0$ in acetonitrile.

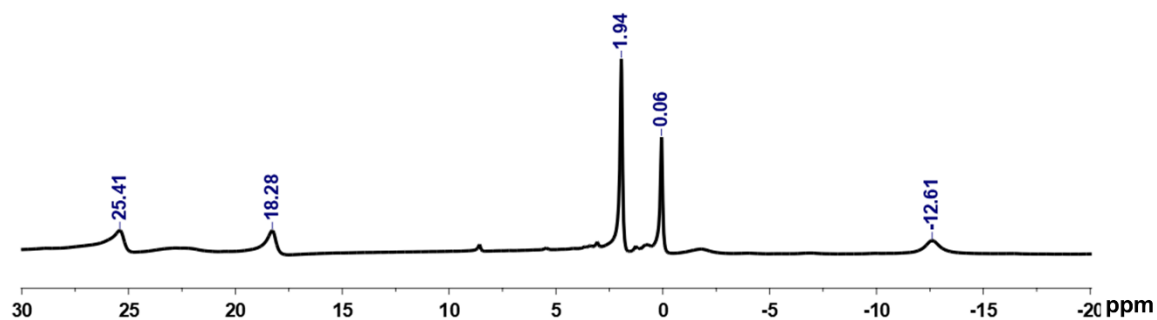


Fig. S10. ^1H NMR (500 MHz, CD_3CN , 21 $^\circ\text{C}$) spectrum of the crude reaction mixture following the addition of 1 equiv of $\text{Pyz}(\text{SiMe}_3)_2$ to $6\text{-V}_6\text{O}_7^0$ in acetonitrile.

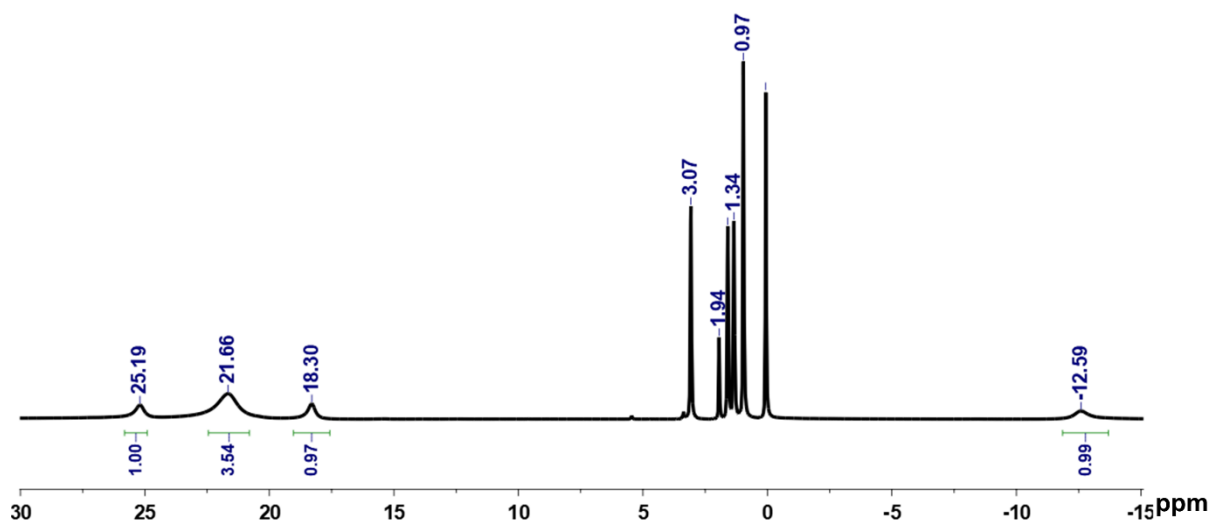


Fig. S11. ^1H NMR (500 MHz, CD_3CN , 21 $^\circ\text{C}$) spectrum of the oxidation of $3\text{-V}_6\text{O}_6\text{OSiMe}_3^{1-}$ with 1.0 equiv of AgOTf ($E_{1/2} = +0.65$ V vs. $\text{Fc}^{+/0}$) in dichloromethane.

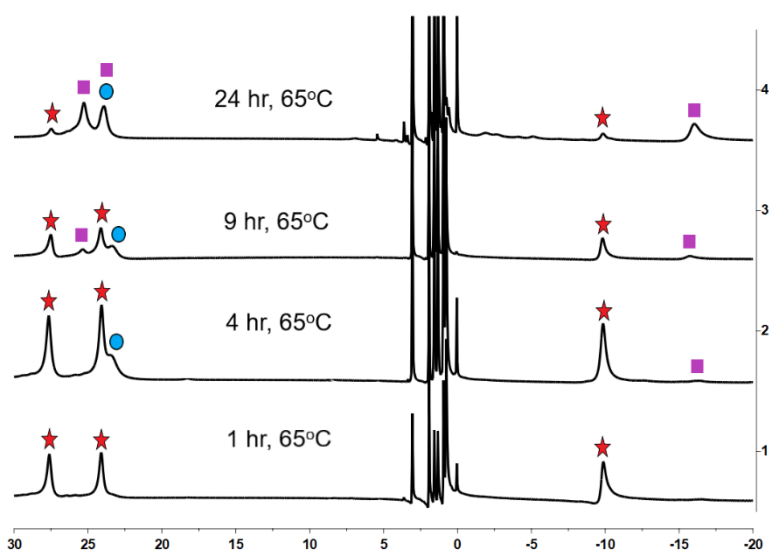


Fig. S12. ^1H NMR (500 MHz, CD_3CN , 21 $^\circ\text{C}$) spectra of the thermal degradation of $3\text{-V}_6\text{O}_6\text{OSiMe}_3^{1-}$ in CD_3CN , 65 $^\circ\text{C}$. The red stars represent $3\text{-V}_6\text{O}_6\text{OSiMe}_3^{1-}$, blue circles stand for $1\text{-V}_6\text{O}_7^{1-}$ and the pink squares denote $2\text{-V}_6\text{O}_6^{1-}$.

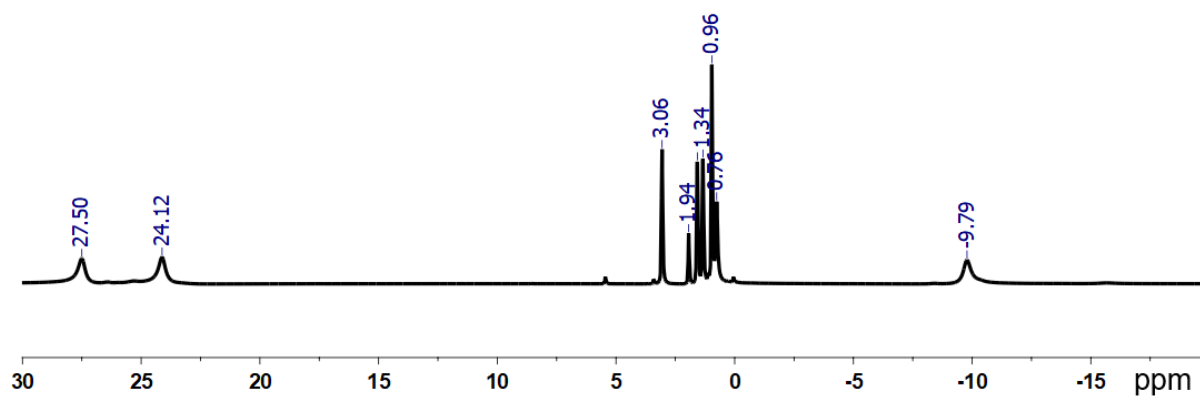


Fig. S13. ¹H-NMR (500 MHz, CD₃CN, 21 °C) spectrum of the reaction following the addition of 0.5 equiv of Pyz(SiMe₃)₂ to **1-V₆O₇¹⁻** in acetonitrile.

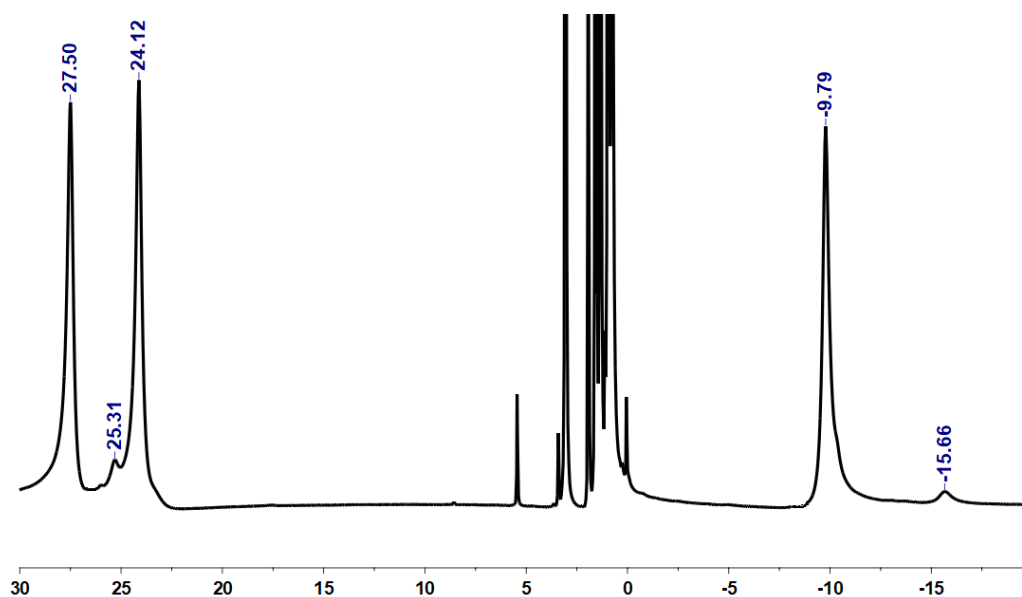


Fig. S14 ¹H-NMR (500 MHz, CD₃CN, 21 °C) spectrum of the reaction following the addition of 0.55 equiv of Pyz(SiMe₃)₂ to **1-V₆O₇¹⁻** in dichloromethane.